

SMAI-JCM
SMAI JOURNAL OF
COMPUTATIONAL MATHEMATICS

Discrete analysis of Schwarz
waveform relaxation for a diffusion
reaction problem with discontinuous
coefficients

SIMON CLEMENT, FLORIAN LEMARIÉ & ERIC BLAYO

Volume 8 (2022), p. 99-124.

http://smai-jcm.centre-mersenne.org/item?id=SMAI-JCM_2022__8__99_0

© Société de Mathématiques Appliquées et Industrielles, 2022

Certains droits réservés.



Publication membre du

Centre Mersenne pour l'édition scientifique ouverte

<http://www.centre-mersenne.org/>

Soumission sur <https://smai-jcm.centre-mersenne.org/ojs/submission>



Discrete analysis of Schwarz waveform relaxation for a diffusion reaction problem with discontinuous coefficients

SIMON CLEMENT¹
FLORIAN LEMARIÉ¹
ERIC BLAYO¹

¹ Univ. Grenoble Alpes, Inria, CNRS, Grenoble INP, LJK, Grenoble, France

E-mail address: simon.clement@grenoble-inp.org

E-mail address: florian.lemarie@inria.fr

E-mail address: eric.blayo@univ-grenoble-alpes.fr.

Abstract. In this paper, we investigate the effect of the space and time discretisation on the convergence properties of Schwarz Waveform Relaxation (SWR) algorithms. We consider a reaction-diffusion problem with discontinuous coefficients discretised on two non-overlapping domains with several numerical schemes (in space and time). A methodology to determine the rate of convergence of the classical SWR method with standard interface conditions (Dirichlet-Neumann or Robin-Robin) accounting for discretisation errors is presented. We discuss how such convergence rates differ from the ones derived at a continuous level (i.e. assuming an exact discrete representation of the continuous problem). In this work we consider a second-order finite difference scheme and a finite volume scheme based on quadratic spline reconstruction in space, combined with either a simple backward Euler scheme or a two-step “Padé” scheme (resembling a Diagonally Implicit Runge Kutta scheme) in time. We prove those combinations of space-time schemes to be unconditionally stable on bounded domains. We illustrate the relevance of our analysis with specifically designed numerical experiments.

2020 Mathematics Subject Classification. 65B99, 65L12, 65M12.

Keywords. Schwarz methods, Waveform relaxation, Semi-discrete.

1. Introduction

Schwarz Waveform Relaxation (SWR) methods [e.g. 14] are widely used in scientific computing for the parallel resolution of numerical models. These iterative methods have proved to be quite efficient, their performances being closely linked to a proper optimisation of their convergence rate. This convergence speed can indeed be improved thanks to several levers, in particular by designing more or less sophisticated interface conditions and by optimising their associated degrees of freedom (e.g. the weight between the Dirichlet and Neumann components within Robin interface conditions, or a relaxation parameter within Dirichlet-Neumann interface conditions). However the actual performances obtained in numerical experiments may be not as good as expected, and several recent studies [e.g. 1, 17, 31] showed that this can be attributed to the effect of the numerical discretisation. As a matter of fact, working at a continuous level neglects the impact of this discretisation, that may be rather significant. On the other hand, taking into account the discretised form of the equations for the optimisation of the convergence obviously reduces the scope of the results and their generality.

In the present paper, we address this optimisation of SWR methods at the discrete level in the context of 1-D diffusion-reaction equations. Such equations are relevant in many fields of application. For example (this was our initial motivation), they can be seen as a simplified formulation of the oceanic and atmospheric thermodynamics in the vicinity of the air-sea interface [e.g. 19], hence as a

This work was supported by the French national research agency through the ANR project “COCOA” (COmprehensive Coupling approach for the Ocean and the Atmosphere), grant ANR-16-CE01-0007. Florian Lemarié appreciates the funding from the SHOM/DGA under grant agreement No 19CP07.

toy model for ocean-atmosphere coupling. But more generally, these equations are also relevant for applications in porous media, electrochemistry, biology, electrical circuit simulations, etc [7, 26].

The diffusion-reaction equations have been widely studied in the context of Schwarz domain decomposition methods (e.g. [8, 11, 13, 24]). However the discrete optimisation of SWR method for these equations has been few addressed yet to our knowledge: the specific case of discrete duality finite volumes with backward Euler time discretisation has been investigated in [5] and [6], while complementary results are presented in the stationary case in [12, 15]. [29] addressed the semi-discrete (i.e. continuous in time) optimisation problem for second-order central and fourth-order compact finite differences, and [30] extended this work to the discrete case with a θ -scheme in time combined with second-order central finite differences in space. However, the analysis excludes a multi-physics setting and the optimisation requires overlapping domains.

Our aim here is to complement those preceding papers by studying the case of several discretisation schemes commonly used in the context of ocean-atmosphere modelling, and trying to take a step back to be fairly general in our methodology and conclusions. Section 2 presents our model problem, and briefly recalls about the SWR algorithm and its convergence rate computed from the continuous equations. Section 3 introduces the two time schemes (backward Euler and Diagonally Implicit Runge Kutta - DIRK) and the two space schemes (second-order central finite difference, and a finite volume scheme based on quadratic spline reconstruction) that we consider. The analytical expression of the semi-discrete convergence rate is computed for Dirichlet-Neumann and for Robin-Robin interface conditions. In Section 4, we prove the stability of the discrete schemes, and study the discrete convergence rate and the interactions between the discretisations in time and space. Then (Section 5), the theoretical speeds of convergence predicted by these continuous, semi-discrete and discrete analyses are compared in actual numerical experiments. We will see that significant differences may appear and emphasize the peculiar role of a centering operator involved in multi-step time schemes.

2. Model problem and Schwarz waveform relaxation algorithm

2.1. Model problem

As indicated previously, the model problem that will be considered in this paper is a reaction-diffusion problem, that reads:

$$\partial_t u_1 + (r - \nu_1 \partial_x^2) u_1 = f_1 \quad (x, t) \in (-\infty, 0) \times]0, T] \quad (2.1a)$$

$$\partial_t u_2 + (r - \nu_2 \partial_x^2) u_2 = f_2 \quad (x, t) \in (0, +\infty) \times]0, T] \quad (2.1b)$$

$$u_1(x, 0) = u_{1,0}(x) \quad x \in (-\infty, 0) \quad (2.1c)$$

$$u_2(x, 0) = u_{2,0}(x) \quad x \in (0, +\infty) \quad (2.1d)$$

$$u_1(0^-, t) = u_2(0^+, t) \quad t \in [0, T] \quad (2.1e)$$

$$\nu_1 \partial_x u_1(0^-, t) = \nu_2 \partial_x u_2(0^+, t) \quad t \in [0, T] \quad (2.1f)$$

where ν_1, ν_2, r are given positive constants. For the sake of simplicity we consider the same damping rate r in the two subdomains, but it is straightforward to extend our results to the case with two different values.

2.2. Schwarz waveform relaxation algorithm

To solve the coupled problem (2.1), a Schwarz waveform relaxation (SWR) algorithm can be set. Such algorithms are well-known and widely used in scientific computing, at least for domain decomposition problems [e.g. 23]. They are also particularly well-suited for coupled problems, since they

can naturally handle differences in the continuous formulations of the models to be coupled (dimensions, equations...) as well as in their discrete formulations (discretisation techniques, space and time steps...). A SWR algorithm applied to (2.1) reads

$$\partial_t u_1^k + (r - \nu_1 \partial_x^2) u_1^k = f_1 \quad (x, t) \in (-\infty, 0) \times]0, T] \quad (2.2a)$$

$$u_1^k(x, 0) = u_{1,0}(x) \quad x \in (-\infty, 0) \quad (2.2b)$$

$$\mathcal{B}_1 u_1^k(0^-, t) = \mathcal{B}_2 u_2^{k-1}(0^+, t) \quad t \in [0, T] \quad (2.2c)$$

then

$$\partial_t u_2^k + (r - \nu_2 \partial_x^2) u_2^k = f_2 \quad (x, t) \in (0, +\infty) \times]0, T] \quad (2.3a)$$

$$u_2^k(x, 0) = u_{2,0}(x) \quad x \in (0, +\infty) \quad (2.3b)$$

$$\mathcal{C}_2 u_2^k(0^+, t) = \mathcal{C}_1 u_1^k(0^-, t) \quad t \in [0, T] \quad (2.3c)$$

where $k \geq 1$ is an iteration index, and where $u_2^0(0^+, t)$ is chosen arbitrarily, or using previous calculations. This iteration loop is repeated until convergence of the sequences $(u_1^k)_k$ and $(u_2^k)_k$. The interface operators \mathcal{B}_j and \mathcal{C}_j ($j = 1, 2$) are chosen such that (2.2) and (2.3) are well-posed, and that satisfying both relations $\mathcal{B}_1 u_1(0^-, t) = \mathcal{B}_2 u_2(0^+, t)$ and $\mathcal{C}_2 u_2(0^+, t) = \mathcal{C}_1 u_1(0^-, t)$ is equivalent to (2.1e) and (2.1f). This ensures that the converged solution satisfies the desired Dirichlet-Neumann interface conditions and thus is the solution of the initial coupled system (2.1).

This algorithm is said to be “multiplicative”, while replacing u_1^k by u_1^{k-1} in (2.3c) would lead to a so-called “parallel” version which requires more iterations to converge but allows for a simultaneous resolution of (2.2) and (2.3) when implemented numerically.

2.3. General form of the continuous convergence rate

In order to study the convergence of the preceding SWR algorithm (2.2)-(2.3), let us introduce the errors $\mathbf{e}_j^k(x, t) = u_j^k(x, t) - u_j(x, t)$ where $u_j(x, t)$ is the solution on domain j of (2.1).. Assuming that the operators \mathcal{B}_j and \mathcal{C}_j are linear, these errors satisfy:

$$\partial_t \mathbf{e}_1^k + (r - \nu_1 \partial_x^2) \mathbf{e}_1^k = 0 \quad (x, t) \in (-\infty, 0) \times]0, T]$$

$$\mathbf{e}_1^k(x, 0) = 0 \quad x \in (-\infty, 0)$$

$$\mathcal{B}_1 \mathbf{e}_1^k(0^-, t) = \mathcal{B}_2 \mathbf{e}_2^{k-1}(0^+, t) \quad t \in [0, T]$$

and

$$\partial_t \mathbf{e}_2^k + (r - \nu_2 \partial_x^2) \mathbf{e}_2^k = 0 \quad (x, t) \in (0, +\infty) \times]0, T]$$

$$\mathbf{e}_2^k(x, 0) = 0 \quad x \in (0, +\infty)$$

$$\mathcal{C}_2 \mathbf{e}_2^k(0^+, t) = \mathcal{C}_1 \mathbf{e}_1^k(0^-, t) \quad t \in [0, T].$$

A time Fourier transform can be performed, assuming that $T \rightarrow +\infty$ and extending \mathbf{e}_j to zero for $t < 0$. This leads to the following ordinary differential equations for the errors $\widehat{\mathbf{e}}_j$ in Fourier space:

$$(i\omega + r) \widehat{\mathbf{e}}_1^k - \nu_1 \partial_x^2 \widehat{\mathbf{e}}_1^k = 0 \quad (x, \omega) \in (-\infty, 0) \times \mathbb{R} \quad (2.4a)$$

$$\mathcal{B}_1 \widehat{\mathbf{e}}_1^k(0^-, \omega) = \mathcal{B}_2 \widehat{\mathbf{e}}_2^{k-1}(0^+, \omega) \quad \omega \in \mathbb{R} \quad (2.4b)$$

and

$$(i\omega + r) \widehat{\mathbf{e}}_2^k - \nu_2 \partial_x^2 \widehat{\mathbf{e}}_2^k = 0 \quad (x, \omega) \in (0, +\infty) \times \mathbb{R} \quad (2.5a)$$

$$\mathcal{C}_2 \widehat{\mathbf{e}}_2^k(0^+, \omega) = \mathcal{C}_1 \widehat{\mathbf{e}}_1^k(0^-, \omega) \quad \omega \in \mathbb{R} \quad (2.5b)$$

where ω is the Fourier frequency. Hence the analytic expressions:

$$\widehat{\mathbf{e}}_1^k(x, \omega) = A_k e^{\mu_1 x} \quad \text{and} \quad \widehat{\mathbf{e}}_2^k(x, \omega) = B_k \mathbf{e}^{-\mu_2 x} \quad (2.6)$$

where μ_j is the square root of $(r + i\omega)/\nu_j$ with positive real part (since $\mathbf{e}_1(x) \rightarrow 0$ for $x \rightarrow -\infty$ and $\mathbf{e}_2(x) \rightarrow 0$ for $x \rightarrow +\infty$).

Convergence factors can thus be defined, equal to $\widehat{\mathbf{e}}_j^k/\widehat{\mathbf{e}}_j^{k-1}$, i.e. A_k/A_{k-1} or B_k/B_{k-1} . The convergence rate of the SWR algorithm is thus equal to the module of these convergence factors. The link between (A_k, B_k) and (A_{k-1}, B_{k-1}) is provided by the interface conditions (2.4b) and (2.5b). In the particular case of Dirichlet-Neumann conditions $\mathbf{e}_1^k(0^-, t) = \mathbf{e}_2^{k-1}(0^+, t)$ and $\nu_2 \partial_x \mathbf{e}_2^k(0^+, t) = \nu_1 \partial_x \mathbf{e}_1^k(0^-, t)$, one gets $A_k = B_{k-1}$ and $-\nu_2 \mu_2 B_k = \nu_1 \mu_1 A_k$, which leads to $A_k/A_{k-1} = B_k/B_{k-1} = -(\nu_1 \mu_1)/(\nu_2 \mu_2) = -\sqrt{\nu_1/\nu_2}$. The convergence rate for infinite domains ¹ is thus

$$\rho_{\text{DN}}^{(c,c)} = \sqrt{\frac{\nu_1}{\nu_2}}. \quad (2.7)$$

The exponent (c, c) means that both the time and space dimensions have been treated in a continuous way to derive (2.7) whereas in the following we will study semi-discrete and fully discrete cases. Similarly, for so-called two-sided Robin interface conditions $\nu_1 \partial_x \mathbf{e}_1^k(0^-, t) + p_1 \mathbf{e}_1^k(0^-, t) = \nu_2 \partial_x \mathbf{e}_2^{k-1}(0^+, t) + p_1 \mathbf{e}_2^{k-1}(0^+, t)$ and $\nu_2 \partial_x \mathbf{e}_2^k(0^+, t) + p_2 \mathbf{e}_2^k(0^+, t) = \nu_1 \partial_x \mathbf{e}_1^k(0^-, t) + p_2 \mathbf{e}_1^k(0^-, t)$, the convergence rate reads:

$$\rho_{\text{RR}}^{(c,c)} = \left| \frac{p_1 - \sqrt{\nu_2} \sqrt{i\omega + r}}{p_1 + \sqrt{\nu_1} \sqrt{i\omega + r}} \frac{p_2 + \sqrt{\nu_1} \sqrt{i\omega + r}}{p_2 - \sqrt{\nu_2} \sqrt{i\omega + r}} \right|.$$

3. Semi-discrete and discrete convergence rates

The discretisation in time (resp. space) uses a step Δt (resp. h) constant across subdomains $j = 1$ and $j = 2$. Time index is noted with the letter n whereas grid points are localised through the index m . The letter k denotes the Schwarz iterate.

From the analysis conducted in this section, we can derive several discrete and semi-discrete convergence rates. In the following, to characterize those convergence rates, we will use the unified notation $\rho_{\text{interface}}^{(\text{time}, \text{space})}$ where “interface” can be either “DN” for Dirichlet-Neumann or “RR” for Robin-Robin, “time” can be “c” for continuous, “BE” for backward Euler or “P2” for the second-order Padé scheme, and “space” is either “c” for continuous, or “FD” for finite difference or “FV” for finite volume. In this section we give the expression of ρ for various combinations of time and space discretisations and interface conditions.

Choosing the discretisation of a continuous problem requires to focus on some desirable properties (e.g. simplicity, accuracy, discrete conservation laws). Two properties arise when using Schwarz methods: the speed of convergence (characterized by ρ) and the difference between the converged solution and a so-called monolithic solution, which solves the problem discretised over the full domain $\Omega_1 \cup \Omega_2$ without any domain decomposition method. The latter difference should not exceed the order of accuracy w.r.t. the continuous problem; apart from that, it may be desirable for additional discrete properties to recover the monolithic solution at convergence up to the precision set to stop the iterations.

3.1. Time discretisation

In this subsection, the objective is to incorporate in the convergence analysis the impact of the time discretisation. The error in time will now be interpreted as a discrete signal $\{e(n)\}_{n=0}^{\infty}$ with constant

¹For finite domains of size H , [27] gives $\rho_{\text{DN}}^{(c,c)} = \sqrt{\frac{\nu_1}{\nu_2}} \left| \coth(-H \sqrt{\frac{r+i\omega}{\nu_1}}) \tanh(H \sqrt{\frac{r+i\omega}{\nu_2}}) \right|$. With our numerical parameters the relative difference with (2.7) is smaller than 1% for $\omega \geq 10^{-3} \text{ s}^{-1}$ without reaction and for all ω if $r \geq 10^{-3} \text{ s}^{-1}$.

sampling Δt ($\Delta t > 0$) such that $e(n)$ approximates the continuous signal $\epsilon(t = n\Delta t)$. To play the role of a discrete equivalent of the Fourier transform used in the continuous analysis (see Sec. 2.3), we use the one-sided \mathcal{Z} -transform [e.g. 4] which is defined as

$$\widehat{e}(z) = \mathcal{Z} \{e(n)\} = \sum_{n=0}^{\infty} e(n)z^{-n}$$

where $z = \exp(s\Delta t)$ with Δt the sampling period and s a complex frequency. In the following we extensively use the property

$$\mathcal{Z} \{e(n+1)\} = z(\mathcal{Z} \{e(n)\} - e(0)) \quad (3.1)$$

knowing that $e(0) = 0$ in our context (the error is initially zero).

3.1.1. One-step time schemes: a change of frequency variable

Time discretisation of our model problem (2.1a)-(2.1b) applied to the errors (i.e. with $f_j = 0$) with a backward Euler scheme gives

$$\frac{e(n+1) - e(n)}{\Delta t} + (r - \nu\partial_x^2)e(n+1) = 0. \quad (3.2)$$

After a \mathcal{Z} -transform and using property (3.1), the semi-discrete equation (3.2) becomes

$$\left(\frac{z-1}{z\Delta t}\right)\widehat{e}(z) + (r - \nu\partial_x^2)\widehat{e}(z) = 0. \quad (3.3)$$

For one-step time schemes, using a \mathcal{Z} -transform instead of a Fourier transform is equivalent to performing a change of variable: the Fourier variable $s = i\omega$ is approximated in the \mathcal{Z} -domain by a s_d^{time} . For the backward Euler scheme it is obvious from (3.3) that $s_d^{\text{BE}}(z) = \frac{z-1}{z\Delta t}$. Once the approximation s_d associated to the temporal discretisation of interest has been found, the rest of the convergence analysis follows the same steps as the one in the continuous case and convergence rates accounting for the time discretisation can be derived. However this methodology only works for one-step time schemes using two time levels like Euler (forward or backward) or Crank-Nicholson, and for one-step time schemes using more time levels like Leapfrog. For more advanced time integration methods, for example used for realistic simulations of geophysical flows [e.g. 20, 28], the determination of convergence rates in the semi-discrete case is significantly more complicated, as shown in the next subsection.

3.1.2. A two-step time scheme

The analyses of two-step time schemes feature higher-order \mathcal{Z} -transformed differential equations. Another specificity of multiple-step time schemes is the time interpolation operator providing boundary and interface conditions to the intermediate steps. A similar temporal operator also appears when considering differing time steps [22], and has a significant impact on the convergence rate of Schwarz iterations.

Determination of the semi-discrete errors. We now consider the ‘‘Pad e’’ two-step (P2) scheme proposed in [21] and [28] which, when applied to our model problem for the errors and reformulated, reads

$$\left(1 + \beta\Delta t \left(r - \nu\partial_x^2\right)\right) e^* = \left(1 - (1 - 2\beta)\Delta t \left(r - \nu\partial_x^2\right)\right) e(n) \quad (3.4a)$$

$$\left(1 + \beta\Delta t \left(r - \nu\partial_x^2\right)\right) e(n+1) = e^* \quad (3.4b)$$

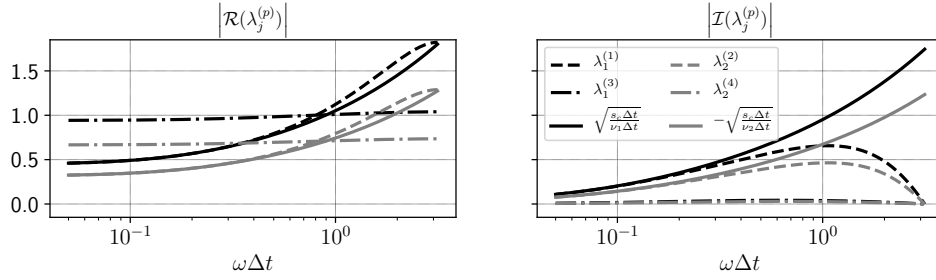


FIGURE 3.1. Absolute value of the real (left) and imaginary (right) parts of the four complex roots of the characteristic equation associated with the Padé time scheme with respect to $\omega\Delta t$. The non-dimensional frequency variable $\omega\Delta t$ naturally appears when dealing with time discretisations. The roots in the continuous case are also reported (solid lines). Parameter values are $\nu_1\Delta t = 0.5 \text{ m}^2$, $\nu_2\Delta t = 1 \text{ m}^2$, $r\Delta t = 0.1$ and $\omega\Delta t \leq \pi$.

with $\beta = 1 + 1/\sqrt{2}$. This scheme, implemented in the atmospheric model of the European Centre for Medium-Range Weather Forecasts (ECMWF), has the property to be second-order accurate, unconditionally stable and “monotonic damping” (i.e. shortest resolved scales are always more damped than the larger ones). This last property is not satisfied by a Crank-Nicolson scheme, which explains why this scheme is seldom used in “real-world” simulations. In a multiple step scheme like (3.4), a discrete frequency $s_d \in \mathbb{C}$ does not naturally appear. Indeed, combining the \mathcal{Z} -transforms of (3.4a) and (3.4b), we obtain

$$\left(z \left(1 + \beta\Delta t \left(r - \nu\partial_x^2 \right) \right)^2 - \left(1 - (1 - 2\beta)\Delta t \left(r - \nu\partial_x^2 \right) \right) \right) \hat{e}(x) = 0 \quad (3.5)$$

where, unlike (3.3), derivatives with orders higher than that of the original equation are present. By analogy with the one-step case, we can rearrange (3.5) as $\left(s_d^{\text{P2}} + r - \nu\partial_x^2 \right) \hat{e} = 0$ to find that s_d^{P2} corresponds to the following differential operator:

$$s_d^{\text{P2}} = s_d^{\text{BE}} + \Delta t(r - \nu\partial_x^2) \left((2\beta - 1) s_d^{\text{BE}} + \beta^2(r - \nu\partial_x^2) \right)$$

where $s_d^{\text{BE}} = \frac{z-1}{z\Delta t}$ is defined in §3.1.1. In multiple-step schemes, even if s_d takes the form of a differential operator and not of a complex scalar, a discrete analysis can nevertheless be pursued. However having no representation of the time discretisation as a simple change of variable means that the temporal scheme contribution to the convergence factor cannot be separated from the space scheme contribution. In the continuous-in-space case, we solve the fourth-order ordinary differential equation (3.5) whose solutions have general form $\hat{e}(x) = \sum_{p=1}^4 c^{(p)} \exp(\lambda^{(p)}x)$ with $\lambda^{(p)}$ the complex roots of the associated characteristic equation. If we note $\lambda^{(1)}, \lambda^{(2)}, \lambda^{(3)}, \lambda^{(4)}$ respectively $\lambda_{(+,-)}, \lambda_{(-,-)}, \lambda_{(+,+)}, \lambda_{(-,+)}$, the $\lambda^{(p)}$'s are

$$\lambda_{(\pm,\pm)} = \pm \frac{1}{\beta\sqrt{2\Delta t\nu}} \sqrt{z^{-1} + 2\beta\Delta t s_d^{\text{BE}} + 2\beta^2\Delta t r \pm \sqrt{z^{-1}} \sqrt{z^{-1} + 4\beta(1-\beta)\Delta t s_d^{\text{BE}}}}$$

and the semi-discrete form of the errors is obtained. Two of the roots ($\lambda^{(2)}$ and $\lambda^{(4)}$) have a negative real part and the two others ($\lambda^{(1)}$ and $\lambda^{(3)}$) have a positive real part. The evolution of $\lambda^{(p)}$ with respect to $\omega\Delta t$ is plotted in Figure 3.1.

3.1.3. *Semi-Discrete convergence rates*

In the following we use the subscript j to distinguish the two subdomains. The boundary conditions at infinity lead to $c_1^{(2)} = c_1^{(4)} = 0$ and $c_2^{(1)} = c_2^{(3)} = 0$ and thus

$$\begin{aligned}\widehat{e}_1(x) &= c_1^{(1)} \exp(\lambda_1^{(1)}x) + c_1^{(3)} \exp(\lambda_1^{(3)}x), & x \in \Omega_1 \\ \widehat{e}_2(x) &= c_2^{(2)} \exp(\lambda_2^{(2)}x) + c_2^{(4)} \exp(\lambda_2^{(4)}x), & x \in \Omega_2\end{aligned}\quad (3.6)$$

where $\Omega_1 = \mathbb{R}_-$ and $\Omega_2 = \mathbb{R}_+$. At this point we have four coefficients to set but only two relations provided by the transmission conditions (either Dirichlet-Neumann or Robin-Robin).

To close this system, it is necessary to provide interface conditions to e^* in (3.4). In the time domain and in the Dirichlet-Neumann case, those interface conditions are $e_1^*(x=0) = e_2(t=t^*, x=0)$ (with $t^* = (n+1-\beta)\Delta t = (n-1/\sqrt{2})\Delta t$) for subdomain $j=1$ and $\nu_2\partial_x e_2^*(x=0) = \nu_1\partial_x e_1(t=t^*, x=0)$ for subdomain $j=2$. We note γ the frequency operator used to center the appropriate values at time t^* . This interpolation or extrapolation operator γ will impact the convergence rate: the choice of γ is discussed below in the present subsection. Considering Dirichlet-Neumann interface conditions, the remaining coefficients in (3.6) are thus determined using the following conditions

$$\widehat{e}_1^k(x=0, z) = \widehat{e}_2^{k-1}(x=0, z) \quad (3.7a)$$

$$\nu_2\partial_x \widehat{e}_2^k(x=0, z) = \nu_1\partial_x \widehat{e}_1^k(x=0, z) \quad (3.7b)$$

$$\left(1 + \Delta t\beta(r - \nu_1\partial_x^2)\right) z\widehat{e}_1^k(x=0, z) = \gamma(z)\widehat{e}_2^{k-1}(x=0, z) \quad (3.7c)$$

$$\nu_2\left(1 + \Delta t\beta(r - \nu_2\partial_x^2)\right) z\partial_x \widehat{e}_2^k(x=0, z) = \gamma(z)\nu_1\partial_x \widehat{e}_1^k(x=0, z) \quad (3.7d)$$

where (3.4b) was used to treat the term $e_j^*(x=0)$. Combining (3.7) and (3.6), we get after some algebra:

$$\begin{aligned}c_{1,k}^{(1)} &= (1 - \tilde{\gamma})\left(c_{2,k}^{(2)} + c_{2,k}^{(4)}\right) \\ c_{1,k}^{(3)} &= \tilde{\gamma}\left(c_{2,k}^{(2)} + c_{2,k}^{(4)}\right) \\ \nu_2c_{2,k}^{(2)}\lambda_2^{(2)} &= (1 - \tilde{\gamma})\nu_1\left(c_{1,k-1}^{(1)}\lambda_1^{(1)} + c_{1,k-1}^{(3)}\lambda_1^{(3)}\right) \\ \nu_2c_{2,k}^{(4)}\lambda_2^{(4)} &= \tilde{\gamma}\nu_1\left(c_{1,k-1}^{(1)}\lambda_1^{(1)} + c_{1,k-1}^{(3)}\lambda_1^{(3)}\right)\end{aligned}\quad (3.8)$$

where

$$\tilde{\gamma} = \frac{z\left(1 + \beta\Delta t\left(r - \nu_1\left(\lambda_1^{(1)}\right)^2\right)\right) - \gamma}{(1/\beta)\sqrt{1 + 4\beta(1-\beta)}(z-1)} = \frac{z\left(1 + \beta\Delta t\left(r - \nu_2\left(\lambda_2^{(2)}\right)^2\right)\right) - \gamma}{(1/\beta)\sqrt{1 + 4\beta(1-\beta)}(z-1)}$$

$\tilde{\gamma}$ represents a weighted difference between two ways to estimate $e_j(x=0, t=t^*)$: either via a time interpolation/extrapolation (by operator γ) or via the second step of the time scheme (3.4), represented by $z\left(1 + \beta\Delta t\left(r - \nu_j\lambda_j^2\right)\right)$. From (3.8) we can deduce a convergence rate defined here as

$$\rho_{\text{DN}}^{(\text{P2,c})} = \left|\varrho_{\text{DN}}^{(\text{P2,c})}\right| = \left|\frac{\nu_1\partial_x \widehat{e}_1^k}{\nu_1\partial_x \widehat{e}_1^{k-1}}\right| \text{ with}$$

$$\varrho_{\text{DN}}^{(\text{P2,c})} = \frac{c_{1,k}^{(1)}\lambda_1^{(1)} + c_{1,k}^{(3)}\lambda_1^{(3)}}{c_{1,k-1}^{(1)}\lambda_1^{(1)} + c_{1,k-1}^{(3)}\lambda_1^{(3)}} = \varrho_{\text{DN}}^{(\text{c,c})} \sqrt{\frac{\nu_1}{\nu_2}} \left(\lambda_1^{(1)}(1 - \tilde{\gamma}) + \lambda_1^{(3)}\tilde{\gamma}\right) \left(\frac{1 - \tilde{\gamma}}{\lambda_2^{(2)}} + \frac{\tilde{\gamma}}{\lambda_2^{(4)}}\right).$$

Choosing γ for multi-step time schemes. When implementing a Schwarz method with multi-step time scheme, a special attention should be paid to the choice of the operator of projection onto the intermediate steps. In the case of the Padé time scheme, a first-order extrapolation from the current times ($\gamma_{\text{extr}} = z(1 - \beta) + \beta$, which corresponds to the weights $1 - \beta$ at t^{n+1} and β at t^n) suffices to guarantee a second-order accuracy of the solution.

Once the desired order of accuracy is attained, one may want to recover the monolithic solution (i.e. the solution that would have been obtained by discretising the problem directly on $\Omega_1 \cup \Omega_2$) to obtain additional discrete properties. This solution can only be obtained if γ perfectly matches the second step of the scheme, resulting in $\tilde{\gamma} = 0$. In such an ideal case, the analysis would be similar to a one-step scheme with the change of variable $s_d^{P2, \tilde{\gamma}=0} = \frac{1}{2\beta^2 \Delta t} (2\beta + (1 - 2\beta) z^{-1} - \sqrt{z^{-1}} \sqrt{z^{-1} + 4\beta(1 - \beta) \Delta t s_d^{\text{BE}}})$ and the operator of projection would be $\gamma^{\tilde{\gamma}=0}(z) = 1 - \frac{1}{2\beta} \left(1 - \sqrt{1 + 4\beta(1 - \beta)(z - 1)} \right)$.

However this operator $\gamma^{\tilde{\gamma}=0}(z)$ is non-local in time: indeed γ is a sum of $z^{\pm p}$ with z^0 representing the current time t_n and $z^{\pm p}$ the time $t_{n \pm p}$. If $\gamma(z)$ is not of this form, then its time counterpart is not local-in-time.

To ensure a small $\tilde{\gamma}$ and a local-in-time γ , a second-order Taylor development of $\gamma^{\tilde{\gamma}=0}(z)$ at $z = 1$ can be made: $\gamma_{\text{imit}}(z) = z - \beta(z - 1) - \beta(\beta - 1)^2(z - 1)^2$. This development is not in general a second-order accurate extrapolation. Indeed, instead of precisely computing the interface condition at $t = t^*$, γ needs to mimic the second step of the time scheme (3.4). A more precise interpolation/extrapolation of $e(t = t^*)$ would thus not give a smaller $\tilde{\gamma}$ because of the error committed by the second step of (3.4).

The choice of γ is crucial for the convergence speed, as can be seen in Figure 3.2 which compares the first-order extrapolation to the Taylor expansion of $\gamma^{\tilde{\gamma}=0}(z)$. This operator is a specific feature of the intermediate steps of multi-step time schemes.

Equivalence with DIRK scheme. The analysed Padé two-step time scheme is equivalent to a Diagonally Implicit Runge-Kutta scheme (DIRK) for space-periodic problems. However, in DIRK schemes as defined in [2]:

$$\begin{aligned} (1 + \beta \Delta t (r - \nu \partial_x^2)) e^{**} &= e(n) \\ (1 + \beta \Delta t (r - \nu \partial_x^2)) e(n + 1) &= e(n) + (1 - \beta) \Delta t (r - \nu \partial_x^2) e^{**} \end{aligned}$$

the intermediate step is not performed in the same way. Consequently, t^{**} is not $\Delta t(n + 1 - \beta)$ but is $t^{**} = \Delta t(n + \beta)$. When considering problems that are non-periodic in space, a Dirichlet interface condition on this e^{**} yields instead of (3.7c):

$$\hat{e}_1^k(x = 0, z) = \gamma(z) \left(1 + \beta \Delta t (r - \nu_1 \partial_x^2) \right) \hat{e}_2^{k-1}(x = 0, z)$$

$\tilde{\gamma}$ and γ hence depend on the intermediate step and the convergence rate may differ from the P2 scheme. However canceling $\tilde{\gamma}$ never leads to a local-in-time $\gamma^{\tilde{\gamma}=0}(z)$ and the above discussion is extendable to other multi-step schemes as long as the steps involve space differentiation.

3.2. Space discretisation

We now consider the semi-discretisation in space at a given location $x = (m + l)h$ of the partial differential equation satisfied by the errors on subdomain Ω_j

$$(\partial_t + r) e_{m+l,j} - \nu_j \partial_x^2 e_j \Big|_{x=x_{m+l}} = 0$$

where we formulate the second-order derivative as a general flux divergence:

$$\nu_j \partial_x^2 e_j \Big|_{x=x_{m+l}} = \frac{\nu_j}{h} \left(\phi_{m+l+\frac{1}{2},j} - \phi_{m+l-\frac{1}{2},j} \right), \quad \text{with } \phi_{m+l+\frac{1}{2},j} \approx \partial_x e_j \Big|_{x=x_{m+l+\frac{1}{2}}} \quad (3.10)$$

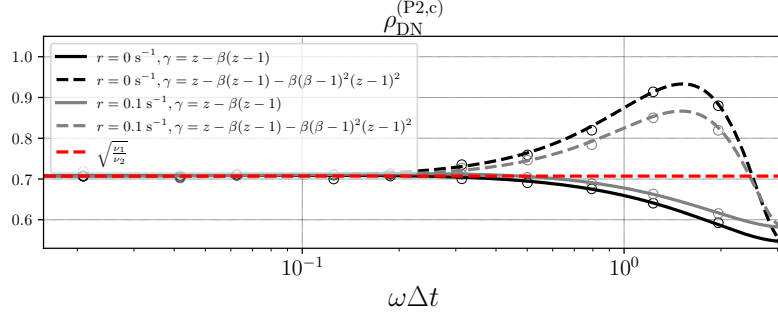


FIGURE 3.2. Convergence rate $\rho_{DN}^{(P2,c)}$ with respect to $\omega\Delta t$ for different choices of the extrapolation function $\gamma(z)$ and different values of the reaction coefficient. Other parameter values are $\nu_1 = 0.5 \text{ m}^2 \text{ s}^{-1}$, $\nu_2 = 1 \text{ m}^2 \text{ s}^{-1}$, $\Delta t = 1 \text{ s}$ and $\omega\Delta t \leq \pi$. The Finite Differences numerical experiment (circles) uses 10^4 vertical levels with a space step $h = 10^{-2}m$ and 300 time steps are performed.

where $l = 0$ or $l = \frac{1}{2}$ depending on the discretisation scheme (see Figure 3.3). In the following we introduce a second-order centered finite difference scheme for which $l = 0$ and a finite volume scheme based on quadratic splines reconstruction for which $l = \frac{1}{2}$. For both schemes we provide the form of the semi-discretised in space error in Fourier space for various interface conditions. Note that the domains are assumed of infinite size ($m \in \mathbb{Z}$) and the numerical experiments that will be presented later will also use a domain large enough for this approximation to be valid.

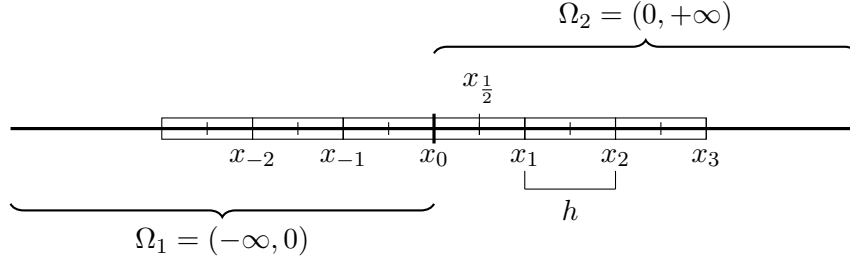


FIGURE 3.3. Computational grid in space for the discretisation in subdomains Ω_1 and Ω_2 with a common interface located at $x = x_0$. For the finite difference scheme presented in Sec. 3.2.1 the solution is computed at integer indices x_m ($m \in \mathbb{Z}$) and fluxes at half indices while for the finite volume scheme in Sec. 3.2.2 control volumes are centered on half indices, i.e. at $x_{m+1/2}$ ($m \in \mathbb{Z}$).

3.2.1. Standard finite difference scheme

We first consider a standard second-order finite difference space scheme for which the approximation of derivatives at cell interfaces is

$$\phi_{m+\frac{1}{2},j}^{\text{FD}} = \frac{e_{m+1,j} - e_{m,j}}{h}.$$

Using (3.10), we easily find that the error at $x = x_m$ satisfies the differential equation

$$(\partial_t + r)e_{m,j} - \frac{\nu_j}{h^2} (e_{m+1,j} - 2e_{m,j} + e_{m,j}) = 0.$$

Denoting $\widehat{e}_{m,j}(s)$ the Fourier transform² of $e_{m,j}(t)$ with $s \in \mathbb{C}$, the error in the frequency domain satisfies

$$(\chi_j + 2)\widehat{e}_{m,j} - (\widehat{e}_{m-1,j} + \widehat{e}_{m+1,j}) = 0, \quad \text{with } \chi_j = \frac{h^2(r+s)}{\nu_j}. \quad (3.11)$$

The general form of the semi-discretised error arising from a finite-difference spatial discretisation is

$$\begin{aligned} \widehat{e}_{m,1}^k &= \alpha_k(s) (\sigma_1^+)^m + \gamma_k(s) (\sigma_1^-)^m \\ \widehat{e}_{m,2}^k &= \beta_k(s) (\sigma_2^-)^m + \varsigma_k(s) (\sigma_2^+)^m \end{aligned}$$

where $\sigma_j^\pm = \frac{1}{2} \left(2 + \chi_j \pm \sqrt{\chi_j(\chi_j + 4)} \right)$. The α_k , γ_k , β_k , and ς_k coefficients are determined using the boundary conditions. The infinite domain assumption leads to $\gamma_k = \varsigma_k = 0$ and thus

$$\widehat{e}_{m,1}^k = \alpha_k(s) (\sigma_1^+)^m, \quad \widehat{e}_{m,2}^k = \beta_k(s) (\sigma_2^-)^m. \quad (3.12)$$

3.2.2. A finite volume scheme based on quadratic spline reconstruction

A finite volume alternative to the standard finite difference scheme is derived in appendix A. This scheme offers the advantage to naturally handle the transmission conditions between the two non-overlapping domains and to guarantee that the converged solution is similar to the monolithic solution of the problem. Among others, [13] also uses a finite volume scheme for the same reasons. This scheme, denoted FV, corresponds to solving the tridiagonal system

$$\frac{1}{6}\phi_{m-1}^{\text{FV}} + \frac{2}{3}\phi_m^{\text{FV}} + \frac{1}{6}\phi_{m+1}^{\text{FV}} = \frac{\bar{u}_{m+\frac{1}{2}} - \bar{u}_{m-\frac{1}{2}}}{h} \quad (3.13)$$

to get ϕ_m^{FV} , and to deduce the second-order derivative via (3.10). In (3.13), $\bar{u}_{m+\frac{1}{2}}$ is defined in a finite-volume sense as $\bar{u}_{m+\frac{1}{2}} = \frac{1}{h} \int_{x_m}^{x_{m+1}} u(x) dx$ with $h = x_{m+1} - x_m$. We then find that the error at $x = x_m$ satisfies the differential equation

$$(\partial_t + r) \left(\frac{1}{6}\phi_{m-1,j}^{\text{FV}} + \frac{2}{3}\phi_{m,j}^{\text{FV}} + \frac{1}{6}\phi_{m+1,j}^{\text{FV}} \right) - \frac{\nu_j}{h^2} (\phi_{m+1,j}^{\text{FV}} - 2\phi_{m,j}^{\text{FV}} + \phi_{m-1,j}^{\text{FV}}) = 0 \quad (3.14)$$

where using coefficients $(\frac{1}{12}, \frac{5}{6})$ instead of $(\frac{1}{6}, \frac{2}{3})$ would give a fourth-order accurate compact scheme [e.g. 18]. For convenience we will formulate here the convergence rate in terms of derivatives $\phi_{m,j}^{\text{FV}}$ instead of the errors $\bar{e}_{m+\frac{1}{2},j}$ themselves. It is straightforward to show that both approaches lead to equivalent results. Unlike in the finite difference case where we applied a Fourier transform on $e_{m,j}(t)$, we apply it here on $\phi_{m,j}^{\text{FV}}(t)$ in (3.14) to obtain the tridiagonal system

$$\left(\frac{\chi_j}{6} - 1 \right) \widehat{\phi}_{m-1,j}^{\text{FV}} + \left(\frac{2\chi_j}{3} + 2 \right) \widehat{\phi}_{m,j}^{\text{FV}} + \left(\frac{\chi_j}{6} - 1 \right) \widehat{\phi}_{m+1,j}^{\text{FV}} = 0 \quad (3.15)$$

where χ_j is defined in (3.11). The roots of the characteristic equation associated to (3.15) are

$$\lambda_j^\pm = \frac{1}{\frac{1}{\chi_j} - \frac{1}{6}} \left(\frac{1}{\chi_j} + \frac{1}{3} \pm \sqrt{\frac{1}{\chi_j} + \frac{1}{12}} \right) \text{ whose Taylor expansion gives}$$

$$\lambda_j^\pm = 1 \pm \sqrt{\frac{r+s}{\nu_j}} h + \frac{h^2}{2} \left(\frac{r+s}{\nu_j} \right) + \mathcal{O}(h^3)$$

²When the time axis is continuous, it should be noted \widehat{e} . However we use the discrete notation \widehat{e} because s can be either the continuous frequency variable or a one-step time scheme change of variable.

showing that λ_j^\pm is an approximation of $e^{\pm\sqrt{\frac{r+s}{\nu_j}}h}$. The infinite domain assumption thus leads to

$$\left(\widehat{\phi}_{m,1}^{\text{FV}}\right)^k = v_k(s) \left(\lambda_1^+\right)^m, \quad \left(\widehat{\phi}_{m,2}^{\text{FV}}\right)^k = \tau_k(s) \left(\lambda_2^-\right)^m \quad (3.16)$$

where $v_k(s) = \sqrt{\frac{s+r}{\nu_1}}\alpha_k(s)$ and $\tau_k(s) = -\sqrt{\frac{s+r}{\nu_2}}\beta_k(s)$ will be determined using the interface conditions.

3.2.3. Interface conditions

The discretisation of the interface conditions will allow to determine the semi-discrete errors in (3.12) and (3.16). In the following we will consider the discretisations of Dirichlet and Neumann interface conditions which also straightforwardly provide the discretisation of Robin interface conditions. We define $\eta_{j,\text{operator}}$ to represent the boundary operator on domain j where ‘‘operator’’ can either be ‘‘dir’’ for a Dirichlet condition or ‘‘neu’’ for a Neumann condition. In a continuous setting, application of the Dirichlet-Neumann interface conditions would lead to

$$\begin{aligned} \eta_{1,\text{dir}}\alpha_k(s) &= \widehat{e}_1^k(0, s) & \eta_{2,\text{dir}}\beta_k(s) &= \widehat{e}_2^k(0, s) \\ \eta_{1,\text{neu}}\alpha_k(s) &= \nu_1\partial_x\widehat{e}_1^k(0, s) & \eta_{2,\text{neu}}\beta_k(s) &= \nu_2\partial_x\widehat{e}_2^k(0, s) \end{aligned}$$

with $\eta_{1,\text{dir}} = \eta_{2,\text{dir}} = 1$, $\eta_{1,\text{neu}} = \sqrt{\nu_1(s+r)}$, and $\eta_{2,\text{neu}} = -\sqrt{\nu_2(s+r)}$. We now derive the discrete counterpart for $\eta_{j,\text{operator}}$ in the finite difference and finite volume cases. In case we work on fluxes $\widehat{\phi}_j^k = \partial_x\widehat{e}_j^k$ rather than directly on the error \widehat{e}_j^k , we would simply have

$$\begin{aligned} \eta_{1,\text{dir}}\alpha_k(s) &= \sqrt{\frac{\nu_1}{s+r}}\widehat{\phi}_1^k(0, s) & \eta_{2,\text{dir}}\beta_k(s) &= -\sqrt{\frac{\nu_2}{s+r}}\widehat{\phi}_2^k(0, s) \\ \eta_{1,\text{neu}}\alpha_k(s) &= \nu_1\widehat{\phi}_1^k(0, s) & \eta_{2,\text{neu}}\beta_k(s) &= \nu_2\widehat{\phi}_2^k(0, s). \end{aligned}$$

Finite differences interface conditions. Due to the grid arrangement we used (see Figure 3.3), the discretisation of the Dirichlet boundary condition in the finite difference case is trivial since a grid point is located on the interface at $x = x_0$. We thus obtain in (3.12) $\widehat{e}_{0,1}^k = \alpha_k(s)$ and therefore $\eta_{1,\text{dir}}^{\text{FD}} = 1$ which corresponds to the continuous case (same applies for subdomain 2). As far as the Neumann boundary condition is concerned, derivatives are naturally located at cell interfaces i.e. a half grid cell inside the domain and the finite difference discretisation requires a specific care. We propose two possible discretisations for the Neumann boundary condition:

- **Strategy #1 (naive discretisation):** assume a Dirichlet-Neumann algorithm with Dirichlet on Ω_1 and Neumann on Ω_2 . For the grid points at $x = x_1$ and $x = x_{-1}$ we have

$$\begin{aligned} \nu_1\partial_x^2 e_1 \Big|_{x=x_{-1}} &= \frac{\nu_1}{h} \left(\widetilde{\phi}_{-\frac{1}{2},1}^{\text{FD}} - \phi_{-\frac{3}{2},1}^{\text{FD}} \right) \\ \nu_2\partial_x^2 e_2 \Big|_{x=x_1} &= \frac{\nu_2}{h} \left(\phi_{\frac{3}{2},2}^{\text{FD}} - \widetilde{\phi}_{\frac{1}{2},2}^{\text{FD}} \right) \end{aligned}$$

where the $\widetilde{\phi}$ fluxes are influenced by interface conditions. On Ω_1 we receive a Dirichlet condition $e_{m=0,1} = e_{\text{int}}$ such that

$$\widetilde{\phi}_{-\frac{1}{2},1}^{\text{FD}} = \frac{e_{\text{int}} - e_{m=-1,1}}{h}$$

and $\nu_1\phi_{-\frac{1}{2},1}^{\text{FD}}$ is sent to subdomain 2 and used as a Neumann condition.

On Ω_2 we have

$$\nu_2\widetilde{\phi}_{\frac{1}{2},2}^{\text{FD}} = \nu_1\widetilde{\phi}_{-\frac{1}{2},1}^{\text{FD}} \quad (3.17)$$

and the Dirichlet condition e_{int} for subdomain Ω_1 is computed as

$$e_{\text{int}} = e_{m=1,2} - h\tilde{\phi}_{\frac{1}{2},2}^{\text{FD}}.$$

- **Strategy #2 (corrected discretisation):** the previous interface discretisation has the drawback to be less accurate than inside the domains. We now derive a second-order accurate discretisation with the additional property of recovering the monolithic solution at convergence of the Schwarz iterations. Starting from the discretisation we would have at $x = x_0$ in the monolithic case:

$$(\partial_t + r) e|_{x=x_0} - \frac{1}{h} \left(\nu_2 \phi_{\frac{1}{2},2}^{\text{FD}} - \nu_1 \phi_{-\frac{1}{2},1}^{\text{FD}} \right) = 0$$

and considering that $e|_{x=x_0} = \frac{1}{2} (e_{m=0,j=1} + e_{m=0,j=2})$ we end up with

$$\nu_1 \phi_{-\frac{1}{2},1}^{\text{FD}} + \frac{h}{2} (\partial_t + r) e_{0,1} = \nu_2 \phi_{\frac{1}{2},2}^{\text{FD}} - \frac{h}{2} (\partial_t + r) e_{0,2} \quad (3.18)$$

as a substitute for (3.17) in the naive case. It is similar to a so-called ghost-point method, but the time derivative in (3.18) will have a significant effect on the convergence. Using the reaction-diffusion equation to replace the time derivative would require to know in a given subdomain the diffusivity used in the other subdomain, which is not always practical.

To obtain unified notations between the naive and the corrected cases, we introduce a parameter κ_c in front of the $\frac{h}{2}$ coefficient in (3.18) such that for $\kappa_c = 0$ we recover the naive Neumann condition (3.17) and for $\kappa_c = 1$ we get the corrected discretisation (3.18).

Now going back to the determination of the $\eta_{j,\text{neu}}$ we apply a Fourier transform on the discretisations (3.17) and (3.18) and use (3.12) to obtain

$$\begin{aligned} \nu_1 \partial_x \hat{e}_1^k \Big|_{x=x_0} &= \nu_1 \frac{\hat{e}_{0,1}^k - \hat{e}_{-1,1}^k}{h} + \kappa_c \frac{h}{2} (s+r) \hat{e}_{0,1}^k = \alpha^k(s) \underbrace{\frac{\nu_1}{h} \left(1 - \frac{1}{\sigma_1^+} + \frac{\kappa_c}{2} \chi_1 \right)}_{\eta_{1,\text{neu}}^{\text{FD}}} \\ \nu_2 \partial_x \hat{e}_2^k \Big|_{x=x_0} &= \nu_2 \frac{\hat{e}_{1,2}^k - \hat{e}_{0,2}^k}{h} - \kappa_c \frac{h}{2} (s+r) \hat{e}_{0,2}^k = \beta^k(s) \underbrace{\frac{\nu_2}{h} \left(\sigma_2^- - 1 - \frac{\kappa_c}{2} \chi_2 \right)}_{\eta_{2,\text{neu}}^{\text{FD}}}. \end{aligned}$$

Finite volume discretisation of interface conditions. In the case of the finite volume discretisation (3.13), the interface conditions are much easier and natural to discretise. Using the notations introduced in appendix A, the error at the interface reads as follows

$$\begin{aligned} e_1(x=0, t) &= \mathcal{S}_{-\frac{1}{2}}(h/2) = \bar{e}_{-\frac{1}{2},1} + \frac{h}{6} \left(\phi_{-1,1}^{\text{FV}} + 2\phi_{0,1}^{\text{FV}} \right) \\ e_2(x=0, t) &= \mathcal{S}_{\frac{1}{2}}(-h/2) = \bar{e}_{\frac{1}{2},2} - \frac{h}{6} \left(\phi_{1,2}^{\text{FV}} + 2\phi_{0,2}^{\text{FV}} \right) \end{aligned}$$

where \mathcal{S} is defined in (A.1) as the spline reconstruction of the solution. Considering the Fourier transform of (A.4) for $m=0$ and $j=1$, we obtain the expression of $\hat{e}_{-\frac{1}{2},1}$, and similarly, using (A.3)

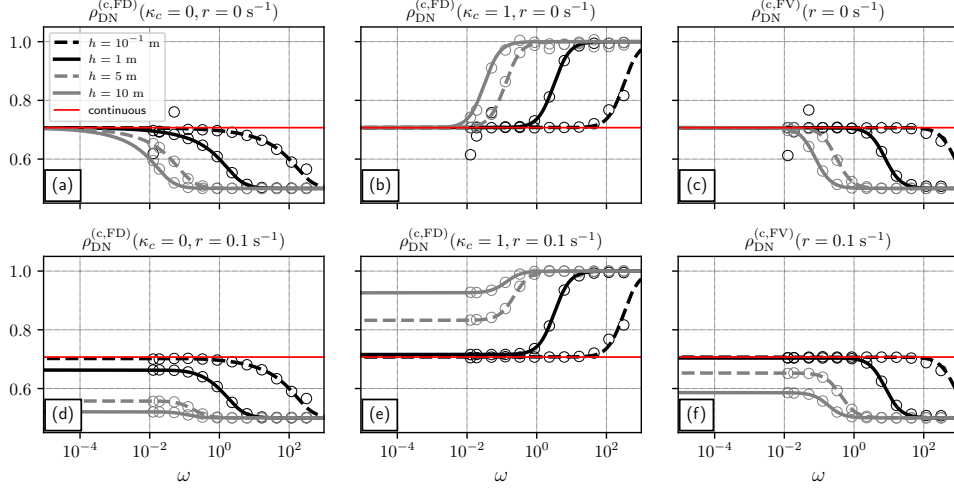


FIGURE 3.4. Convergence rates with Dirichlet-Neumann interface conditions with respect to ω for $s = i\omega$, $\nu_1 = 0.5 \text{ m}^2 \text{ s}^{-1}$, $\nu_2 = 1 \text{ m}^2 \text{ s}^{-1}$. The convergence rates represented correspond to (a) $\rho_{\text{DN}}^{(\text{c,FD})}$ for $\kappa_c = 0$ and $r = 0 \text{ s}^{-1}$, (b) $\rho_{\text{DN}}^{(\text{c,FD})}$ for $\kappa_c = 1$ and $r = 0 \text{ s}^{-1}$, (c) $\rho_{\text{DN}}^{(\text{c,FV})}$ for $r = 0 \text{ s}^{-1}$ (d),(e) and (f) are the same as (a),(b) and (c) but for $r = 0.1 \text{ s}^{-1}$. Results are shown for different values of h : $h = 0.1 \text{ m}$ (black dashed lines), $h = 1 \text{ m}$ (black solid lines), $h = 5 \text{ m}$ (grey dashed lines), and $h = 10 \text{ m}$ (grey solid lines). The convergence rate in the continuous case is represented with red solid lines.

for $m = 0$ and $j = 2$, we obtain $\widehat{e}_{\frac{1}{2},2}^k$. We end up with:

$$\widehat{e}_1^k(0, s) = \left\{ \left(\frac{h}{3} + \frac{h}{\chi_1} \right) (\widehat{\phi}_{0,1}^{\text{FV}})^k + \left(\frac{h}{6} - \frac{h}{\chi_1} \right) (\widehat{\phi}_{-1,1}^{\text{FV}})^k \right\} = \underbrace{\alpha_k(s) \sqrt{\chi_1} \left[\left(\frac{1}{3} + \frac{1}{\chi_1} \right) + \left(\frac{1}{6} - \frac{1}{\chi_1} \right) \frac{1}{\lambda_1^+} \right]}_{\eta_{1,\text{Dir}}^{\text{FV}}}$$

$$\widehat{e}_2^k(0, s) = \left\{ \left(\frac{h}{\chi_2} - \frac{h}{6} \right) (\widehat{\phi}_{1,2}^{\text{FV}})^k - \left(\frac{h}{\chi_2} + \frac{h}{3} \right) (\widehat{\phi}_{0,2}^{\text{FV}})^k \right\} = \underbrace{\beta_k(s) \sqrt{\chi_2} \left[\left(\frac{1}{\chi_2} + \frac{1}{3} \right) - \left(\frac{1}{\chi_2} - \frac{1}{6} \right) \lambda_2^- \right]}_{\eta_{2,\text{Dir}}^{\text{FV}}}.$$

The expressions for $\eta_{j,\text{Dir}}^{\text{FV}}$ thus obtained can be further simplified and are such that $\eta_{j,\text{Dir}}^{\text{FV}} = \sqrt{1 + \frac{\chi_j}{12}}$. As far as the Neumann boundary condition is concerned, since we have constructed the scheme under the constraints $\partial_\xi \mathcal{S}_{1/2}(-h/2) = \phi_{0,2}^{\text{FV}}$ and $\partial_\xi \mathcal{S}_{-1/2}(h/2) = \phi_{0,1}^{\text{FV}}$ (see appendix A) we easily obtain $\eta_{1,\text{neu}} = \sqrt{(s+r)\nu_1} = \frac{\nu_1 \sqrt{\chi_1}}{h}$ and $\eta_{2,\text{neu}} = -\sqrt{(s+r)\nu_2} = -\frac{\nu_2 \sqrt{\chi_2}}{h}$ (i.e. the ones from the continuous case). As mentioned earlier our finite volume discretisation allows to recover at convergence the solution that would have been obtained by a numerical simulation over the union of the two subdomains up to the precision set to stop the iterations.

TABLE 3.1. Summary of the formulation of the $\eta_{j,\text{dir}}$ and $\eta_{j,\text{neu}}$ quantities which characterise the space discretisation through the interface operators. $\kappa_c = 1$ for the corrected FD case and $\kappa_c = 0$ in the naive FD case.

Space setting	$\eta_{1,\text{dir}}$	$\eta_{2,\text{dir}}$	$\eta_{1,\text{neu}}$	$\eta_{2,\text{neu}}$
Finite Volume	$\sqrt{1 + \frac{\chi_1}{12}}$	$\sqrt{1 + \frac{\chi_2}{12}}$	$\frac{\nu_1}{h} \sqrt{\chi_1}$	$-\frac{\nu_2}{h} \sqrt{\chi_2}$
Finite Difference	1	1	$\frac{\nu_1}{2h} \left(\chi_1(\kappa_c - 1) + \sqrt{\chi_1(4 + \chi_1)} \right)$	$\frac{\nu_2}{2h} \left(\chi_2(1 - \kappa_c) - \sqrt{\chi_2(4 + \chi_2)} \right)$
Continuous	1	1	$\frac{\nu_1}{h} \sqrt{\chi_1}$	$-\frac{\nu_2}{h} \sqrt{\chi_2}$

TABLE 3.2. Frequency variables s , which characterise the time discretisation. z can be replaced by $e^{i\omega\Delta t}$. Using a change of variable for a multi-step time scheme would neglect the projection operator γ (see section 3.1.3).

Time setting	s
Backward Euler	$s_d^{\text{BE}} = \frac{z-1}{z\Delta t}$
Padé scheme	$s_d^{\text{P2}} = \frac{z-1}{z\Delta t} - \Delta t \left((2\beta - 1) \frac{z-1}{z\Delta t} \nu (\partial_x^2 - r) - \beta^2 \nu^2 (\partial_x^2 - r)^2 \right)$
Continuous	$s_c = i\omega$

3.2.4. Semi-Discrete convergence rates

We study the semi-discrete in space case where the determination of $\alpha_k(s)$ and $\beta_k(s)$ in (3.12) can be easily done via the $\eta_{j,\text{dir}}$ and $\eta_{j,\text{neu}}$ expressions derived in previous subsection. In the Dirichlet-Neumann case, the transmission conditions lead to

$$\eta_{1,\text{dir}}^{\text{FD}} \alpha_k(s) = \eta_{2,\text{dir}}^{\text{FD}} \beta_k(s) \quad (3.19)$$

$$\eta_{2,\text{neu}}^{\text{FD}} \beta_k(s) = \eta_{1,\text{neu}}^{\text{FD}} \alpha_{k-1}(s) \quad (3.20)$$

and using the specific form of the η_j functions given in Tab. 3.1 we obtain the convergence rate (corresponding here to $|\alpha_k/\alpha_{k-1}|$)

$$\rho_{\text{DN}}^{(\text{c,FD})} = \left| \frac{\eta_{2,\text{dir}}^{\text{FD}} \eta_{1,\text{neu}}^{\text{FD}}}{\eta_{1,\text{dir}}^{\text{FD}} \eta_{2,\text{neu}}^{\text{FD}}} \right| = \left| \varrho_{\text{DN}}^{(\text{c,FD})} \right|, \quad \varrho_{\text{DN}}^{(\text{c,FD})} = \frac{\nu_1}{\nu_2} \left(\frac{\chi_1(\kappa_c - 1) + \sqrt{\chi_1(\chi_1 + 4)}}{\chi_2(1 - \kappa_c) - \sqrt{\chi_2(\chi_2 + 4)}} \right)$$

where we recall that $\chi_j = h^2(s + r)/\nu_j$. For $h \rightarrow 0$ we have

$$\varrho_{\text{DN}}^{(\text{c,FD})} = \sqrt{\frac{\nu_1}{\nu_2}} + (\kappa_c - 1) \frac{h}{2} \left(\sqrt{\frac{\nu_1}{\nu_2}} - 1 \right) \sqrt{\frac{s+r}{\nu_2}} + \mathcal{O}(h^2)$$

and thus $\rho_{\text{DN}}^{(\text{c,FD})}$ is a first-order (resp. second-order) approximation of the convergence rate $\rho_{\text{DN}}^{(\text{c,c})}$ in the continuous case for $\kappa_c = 0$ (resp. $\kappa_c = 1$). The Taylor expansion of $\varrho_{\text{DN}}^{(\text{c,FD})}$ suggests that the impact of numerical errors is small when ν_1 is close to ν_2 and ν_2 is large because the leading order term is scaled by $\frac{\sqrt{\nu_1} - \sqrt{\nu_2}}{\nu_2}$. In other situations the numerical results may deviate significantly from the continuous

analysis as shown in Figure 3.4. Moreover, whatever the parameter values, $\lim_{\omega \rightarrow \infty} \varrho_{\text{DN}}^{(\text{c,FD})} \Big|_{\kappa_c=1} = 1$ (with $\omega = \text{Im}(s)$) such that we can anticipate poor performances with finite differences for high temporal

frequencies. Figure 3.4 illustrates this aspect. On the other hand, $\lim_{\omega \rightarrow \infty} \varrho_{\text{DN}}^{(\text{c,FD})} \Big|_{\kappa_c=0} = \frac{\nu_1}{\nu_2}$ which means that the algorithm converges faster (if $\nu_1 < \nu_2$) for high frequencies.

In the continuous analysis, the reaction coefficient r does not appear in the convergence factor which depends only on the diffusion coefficients ν_j ($j = 1, 2$), see (2.7). However in the semi-discretised in space case with finite difference, the following asymptotes for low frequencies can be found:

$$\lim_{\omega \rightarrow 0} \varrho_{\text{DN}}^{(\text{c,FD})} \Big|_{\kappa_c=1} = \sqrt{\frac{\nu_1}{\nu_2}} \left(\frac{1 + \frac{rh^2}{4\nu_1}}{1 + \frac{rh^2}{4\nu_2}} \right), \quad \lim_{\omega \rightarrow 0} \varrho_{\text{DN}}^{(\text{c,FD})} \Big|_{\kappa_c=0} = \sqrt{\frac{\nu_1}{\nu_2}} \frac{\sqrt{1 + \frac{rh^2}{4\nu_1}} - \sqrt{\frac{rh^2}{4\nu_1}}}{\sqrt{1 + \frac{rh^2}{4\nu_2}} - \sqrt{\frac{rh^2}{4\nu_2}}}$$

meaning that the discretisation affects the convergence factor even at lower frequencies compared to the continuous case. In particular, assuming that $\nu_1 < \nu_2$ we have $\left(\frac{1 + \frac{rh^2}{4\nu_1}}{1 + \frac{rh^2}{4\nu_2}} \right) > 1$. The convergence is thus slower and increasing r slows it down with the corrected FD discretisation. With the naive FD discretisation, the convergence is faster than predicted by the continuous analysis since $\frac{\sqrt{1 + \frac{rh^2}{4\nu_1}} - \sqrt{\frac{rh^2}{4\nu_1}}}{\sqrt{1 + \frac{rh^2}{4\nu_2}} - \sqrt{\frac{rh^2}{4\nu_2}}} < 1$, and increasing r accelerates the convergence. The impact of the reaction coefficient on the convergence rate is illustrated in Figure 3.4.

In the finite volume case, (3.19) and (3.20) also apply, and

$$\rho_{\text{DN}}^{(\text{c,FV})} = \left| \frac{\eta_{1,\text{neu}}^{\text{FV}} \eta_{2,\text{dir}}^{\text{FV}}}{\eta_{2,\text{neu}}^{\text{FV}} \eta_{1,\text{dir}}^{\text{FD}}} \right| = \left| \varrho_{\text{DN}}^{(\text{c,FV})} \right|, \quad \varrho_{\text{DN}}^{(\text{c,FV})} = \frac{\nu_1 \sqrt{\frac{\chi_1}{12 + \chi_1}}}{\nu_2 \sqrt{\frac{\chi_2}{12 + \chi_2}}}.$$

$\varrho_{\text{DN}}^{(\text{c,FV})}$ is a second-order approximation of $\sqrt{\nu_1/\nu_2}$, since

$$\varrho_{\text{DN}}^{(\text{c,FV})} = \sqrt{\frac{\nu_1}{\nu_2}} + \frac{h^2}{24} \left(\frac{\nu_1 - \nu_2}{\sqrt{\nu_1 \nu_2}} \right) \left(\frac{s + r}{\nu_2} \right) + \mathcal{O}(h^4).$$

Just like in the finite difference case, the order of magnitude of the leading error term in the Taylor expansion for $h \rightarrow 0$ depends on the parameter values for ν_1 and ν_2 . This is also the case for large values of ω since $\lim_{\omega \rightarrow \infty} \varrho_{\text{DN}}^{(\text{c,FV})} = \frac{\nu_1}{\nu_2}$. Like in the naive FD case, in the FV case the algorithm for $\nu_1 < \nu_2$ will be more efficient for high temporal frequencies than for low frequencies. This is confirmed by Figure 3.4.

The reaction coefficient does not affect the asymptote for large values of ω . However for small values of ω we have

$$\lim_{\omega \rightarrow 0} \varrho_{\text{DN}}^{(\text{c,FV})} = \sqrt{\frac{\nu_1}{\nu_2}} \sqrt{\frac{1 + \frac{h^2 r}{12\nu_2}}{1 + \frac{h^2 r}{12\nu_1}}}$$

which is systematically smaller than $\sqrt{\nu_1/\nu_2}$ for $\nu_1 < \nu_2$ as seen in Figure 3.4. Moreover, with both discretisations $\varrho_{\text{DN}}^{(\text{c,c})}$ is obtained when $\chi_j \rightarrow 0$. Consequently if $s + r \rightarrow 0$ the continuous convergence rate is recovered even when using a large h .

4. Discrete case

4.1. Stability analysis

In the following, we investigate the stability of the various combinations between the space and time discretisations. To this aim, we consider a Dirichlet condition on the external boundaries of the individual subproblems and Robin conditions at interface. It will thus be straightforward to extend the

results to a Dirichlet or a Neumann interface condition. The subscript j is omitted as the stability does not depend on it. To describe the space discretisations, we introduce two tridiagonal matrices $\mathbf{Y}^{\{\text{FD},\text{FV}\}}$ and two tridiagonal matrices $\mathbf{D}^{\{\text{FD},\text{FV}\}}$ such that both discretisations read in matrix form

$$\left((\partial_t + r)\mathbf{Y} - \frac{\nu}{h^2}\mathbf{D} \right) \mathbf{x} = \mathbf{c}$$

where \mathbf{x} represents the variable u with the finite difference discretisation and the variable ϕ when using finite volumes. \mathbf{c} has no effect on the stability, and consists of the possible forcing and contributions from the boundary and interface conditions.

$$\mathbf{Y}^{\text{FD}} = \begin{pmatrix} \frac{1}{2}\kappa_c & & & & \\ & 1 & & 0 & \\ & & \ddots & & \\ & & & 1 & \\ & 0 & & & 0 \end{pmatrix}, \mathbf{D}^{\text{FD}} = \begin{pmatrix} -(\frac{h}{\nu}\tilde{p} + 1) & 1 & & & \\ & 1 & -2 & 1 & 0 \\ & & \ddots & \ddots & \ddots \\ & & & & -2 & 1 \\ & 0 & & & & 0 & -1 \end{pmatrix} \quad (4.1)$$

and

$$\mathbf{Y}^{\text{FV}} = \frac{1}{6} \begin{pmatrix} 2(3 + \frac{h}{\nu}\tilde{p}) & \frac{h}{\nu}\tilde{p} & & & \\ & 1 & 4 & 1 & 0 \\ & & \ddots & \ddots & \ddots \\ & & & 1 & 4 & 1 \\ & 0 & & & 1 & 2 \end{pmatrix}, \mathbf{D}^{\text{FV}} = \begin{pmatrix} -\frac{h\tilde{p}}{\nu} & \frac{h\tilde{p}}{\nu} & & & \\ & 1 & -2 & 1 & 0 \\ & & \ddots & \ddots & \ddots \\ & & & 1 & -2 & 1 \\ & 0 & & & & 1 & -1 \end{pmatrix}. \quad (4.2)$$

\tilde{p} is p_1 in the domain Ω_1 or $-p_2$ in the domain Ω_2 .

4.1.1. Theoretical tools for analysis

The proof of stability relies on the hypothesis that $\tilde{p} \geq 0$ to obtain diagonally dominant matrices. The following propositions will help us proving the stability of both time schemes by providing the sign of the eigenvalues of $(\mathbf{D}^{\text{FD}})^{-1}\mathbf{Y}^{\text{FD}}$ and $(\mathbf{Y}^{\text{FV}})^{-1}\mathbf{D}^{\text{FV}}$.

Proposition 4.1. *For any $l \in \mathbb{C}$ such as $\Re(l) > 0$, $\det(\mathbf{D} - l\mathbf{Y}) \neq 0$ (i.e. $\det(\mathbf{D}^{\text{FV}} - l\mathbf{Y}^{\text{FV}}) \neq 0$ and $\det(\mathbf{D}^{\text{FD}} - l\mathbf{Y}^{\text{FD}}) \neq 0$).*

Proof. Using the hypotheses $\tilde{p} \geq 0$ and $\Re(l) > 0$, we get:

- $\mathbf{D}^{\text{FV}} - l\mathbf{Y}^{\text{FV}}$ is strictly diagonally dominant and is hence non-singular.
- If $\kappa_c = 1$ or $\tilde{p} > 0$, $\mathbf{D}^{\text{FD}} - l\mathbf{Y}^{\text{FD}}$ is also strictly diagonally dominant.
- If $\kappa_c = 0$ and $\tilde{p} = 0$, the first row of $\mathbf{D}^{\text{FD}} - l\mathbf{Y}^{\text{FD}}$ is only weakly diagonally dominant. However the matrix is *weakly chained diagonally dominant* (see e.g. [3]) thus non-singular. ■

Proposition 4.2. *\mathbf{D}^{FD} and \mathbf{Y}^{FV} are non-singular.*

Proof. \mathbf{Y}^{FV} is strictly diagonally dominant and \mathbf{D}^{FD} is weakly chained diagonally dominant. Hence both are non-singular. ■

From now on, the superscript FD or FV will be omitted when a sentence stands for both discretisations.

4.1.2. *Stability of the Backward Euler scheme*

The Backward Euler scheme corresponds to the operation $\mathbf{A}\mathbf{x}^{n+1} = \mathbf{Y}\mathbf{x}^n + \Delta t\mathbf{c}$ where $\mathbf{A} = ((1 + r\Delta t)\mathbf{Y} - \Gamma\mathbf{D})$ and Γ is the parabolic Courant number.

Proposition 4.3. *The Backward Euler scheme is unconditionally stable with FD and FV on a bounded domain with Dirichlet-Robin boundary conditions.*

Proof. It is easy to see that \mathbf{A} is non-singular for $\tilde{p} \geq 0$. Let $\sigma \in \mathbb{C}^*$ be a non-zero eigenvalue of $\mathbf{A}^{-1}\mathbf{Y}$ and \mathbf{v} the associated eigenvector. Then $\sigma\mathbf{A}\mathbf{v} = \mathbf{Y}\mathbf{v}$, i.e. $(\sigma(1 + r\Delta t) - 1)\mathbf{Y}\mathbf{v} = \sigma\Gamma\mathbf{D}\mathbf{v}$. Then:

- \mathbf{v} is an eigenvector of $(\mathbf{Y}^{\text{FV}})^{-1}\mathbf{D}^{\text{FV}}$, with eigenvalue $\lambda = \frac{\sigma(1+r\Delta t)-1}{\Gamma\sigma}$.
- \mathbf{v} is an eigenvector of $(\mathbf{D}^{\text{FD}})^{-1}\mathbf{Y}^{\text{FD}}$, with eigenvalue $1/\lambda$.

We assumed that $\sigma \neq 0$. By definition of λ , $\det(\mathbf{D} - \lambda\mathbf{Y}) = 0$. From proposition 4.1 we get that $\Re(\lambda) \leq 0$, and since $\sigma = \frac{1}{1+r\Delta t-\Gamma\lambda}$, we conclude that $|\sigma| \leq 1$. The moduli of all eigenvalues of $\mathbf{A}^{-1}\mathbf{Y}$ are therefore smaller or equal to 1: the Backward Euler scheme is unconditionally stable for finite differences and for finite volumes (for variable ϕ).

Special attention must be paid to the finite volume scheme if $r = 0$: $\bar{u}_{m+1/2}^n = \bar{u}_{m+1/2}^0 + \frac{\nu}{h} \sum_{i=1}^n (\phi_{m+1}^i - \phi_m^i + \bar{f}_{m+1/2}^i)$. To prove stability we need this serie to be bounded when $\bar{f} = 0$ and the eigenvalues should hence be of modulus strictly smaller than 1 in order to have geometric convergence. However the eigenspace associated to 1 is the kernel of \mathbf{D}^{FV} . In this eigenspace, $\phi_{m+1} - \phi_m = 0$. We hence conclude that the Backward Euler scheme is unconditionally stable also for the variable \bar{u} of finite volumes. \blacksquare

 4.1.3. *Stability of the “Padé” two-step scheme*

The “Padé” two-step time scheme studied in this paper reads:

$$\begin{aligned} (\widetilde{\mathbf{Y}}_\beta - \beta\Gamma\mathbf{D})\mathbf{x}^* &= \left(\widetilde{\mathbf{Y}}_{2\beta-1} - (2\beta-1)\Gamma\mathbf{D} \right) \mathbf{x}^n + \beta\Delta t\mathbf{c}^* - (2\beta-1)\Delta t\mathbf{c}^n \\ (\widetilde{\mathbf{Y}}_\beta - \beta\Gamma\mathbf{D})\mathbf{x}^{n+1} &= \mathbf{Y}\mathbf{x}^* + \beta\Delta t\mathbf{c}^{n+1} \end{aligned}$$

where $\widetilde{\mathbf{Y}}_X = (1 + Xr\Delta t)\mathbf{Y}$ and $\Gamma = \frac{\nu\Delta t}{h^2}$.

Proposition 4.4. *The “Padé” two-step scheme is unconditionally stable with FD and FV on a bounded domain with Dirichlet-Robin boundary conditions.*

Proof. We study the eigenvalues of the matrix

$$\mathbf{A}_P = \left(\widetilde{\mathbf{Y}}_\beta - \beta\Gamma\mathbf{D} \right)^{-1} \mathbf{Y} \left(\widetilde{\mathbf{Y}}_\beta - \beta\Gamma\mathbf{D} \right)^{-1} \left(\widetilde{\mathbf{Y}}_{2\beta-1} - (2\beta-1)\Gamma\mathbf{D} \right).$$

From proposition 4.1:

- we get that all eigenvalues $\lambda \in \mathbb{C}$ of $(\mathbf{Y}^{\text{FV}})^{-1}\mathbf{D}^{\text{FV}}$ are such that $\Re(\lambda) \leq 0$.
- All non-zero eigenvalues $1/\lambda \in \mathbb{C}$ of $(\mathbf{D}^{\text{FD}})^{-1}\mathbf{Y}^{\text{FD}}$ are such that $\Re(\lambda) \leq 0$.

Let $\lambda \in \mathbb{C}$ defined as in one of the two cases above. The associated eigenvector is also an eigenvector of \mathbf{A}_P , with eigenvalue σ given by:

$$\sigma = \frac{1 + (2\beta-1)(r\Delta t - \Gamma\lambda)}{(1 + \beta(r\Delta t - \Gamma\lambda))^2}. \quad (4.3)$$

All the eigenvalues of \mathbf{A}_P correspond to a λ in (4.3) or correspond to the zero eigenvalue of $(\mathbf{D}^{FD})^{-1}\mathbf{Y}^{FD}$. In the latter case, the eigenvectors correspond to the zero eigenvalue of \mathbf{A}_P .

Since Γ and $r\Delta t$ are strictly positive, we can restrain our study to the function $\tilde{\lambda} \mapsto \left| \frac{1+(2\beta-1)\tilde{\lambda}}{(1+\beta\tilde{\lambda})^2} \right|$, where $\tilde{\lambda} = r\Delta t - \Gamma\lambda$ belongs to the right half of the complex plane. A routine calculation returns that for $\beta = 1 + 1/\sqrt{2}$, this function is always strictly smaller than 1, except in $\tilde{\lambda} = 0$.

As for the Backward Euler scheme, the eigenspace associated to $\sigma = 1$ for finite volumes scheme is the kernel of \mathbf{D}^{FV} and we can draw the same conclusion: the Padé two-step time scheme is unconditionally stable. ■

4.2. Convergence rates

In previous subsections we have derived the semi-discrete (either in time or in space) convergence rates of SWR algorithm. Now that we have checked that the various combinations of space and time discretisations are unconditionally stable for bounded domains, the discrete convergence rates can be studied.

In Section 3.1 we mentioned that adding the time-discretisation in the analysis amounts to a change of variable for one-step time schemes (i.e. s in the continuous case is replaced by $s_d(z)$ in the discretised case). We also showed that for a multiple-step time scheme, the convergence factor $\rho_{\text{DN}}^{(\text{P2,space})}$ requires solving a characteristic equation which is fourth order. Because of the lengthy computations involved in the derivation of $\rho_{\text{DN}}^{(\text{P2,FD})}$ and $\rho_{\text{DN}}^{(\text{P2,FV})}$ we do not provide their analytical expressions.

4.2.1. Dirichlet-Neumann boundary conditions

The convergence with Dirichlet-Neumann operators does not directly depend on the discretisation in time itself. Indeed $\rho_{\text{DN}}^{(\text{BE,c})} = \rho_{\text{DN}}^{(\text{c,c})}$ and $\rho_{\text{DN}}^{(\text{P2,c})} = \rho_{\text{DN}}^{(\text{c,c})}$ (provided that $\tilde{\gamma} = 0$). With those transmission operators, changing the value of Δt in a semi-discrete in time convergence rate has no effect, whereas changing it in a fully-discrete case shows the effect of the time scheme on the semi-discrete in space convergence rate.

Figure 4.1 shows the fully-discrete convergence rate for several values of the parabolic Courant number $\Gamma = \nu\Delta t/h^2$. The convergence rate is not much affected by Backward Euler scheme (a, b, c). This is not surprising as the semi-discrete in time and the continuous convergence rates are identical. On the other hand, the Padé time scheme (d, e, f) interacts with the Finite Difference scheme differently when changing the operator γ . In the right column, the reaction coefficient r accelerates the convergence in low frequencies and damps the space-time interactions. We see that leaving aside the operator γ which plays an important role in high frequencies, the discretisation in time modifies only slightly the effect of the semi-discrete analysis in space.

4.2.2. Robin-Robin boundary conditions

Now considering the two-sided Robin-Robin case for one-step time schemes, we obtain the following general expression of the interface conditions:

$$\begin{aligned} p_1\eta_{1,\text{dir}}\alpha_k(s) + \eta_{1,\text{neu}}\alpha_k(s) &= p_1\eta_{2,\text{dir}}\beta_k(s) + \eta_{2,\text{neu}}\beta_k(s) \\ p_2\eta_{2,\text{dir}}\beta_k(s) + \eta_{2,\text{neu}}\beta_k(s) &= p_2\eta_{1,\text{dir}}\alpha_{k-1}(s) + \eta_{1,\text{neu}}\alpha_{k-1}(s). \end{aligned}$$

The convergence rate thus reads:

$$\rho_{\text{RR}} = \left| \frac{(p_2\eta_{1,\text{dir}} + \eta_{1,\text{neu}})(p_1\eta_{2,\text{dir}} + \eta_{2,\text{neu}})}{(p_2\eta_{2,\text{dir}} + \eta_{2,\text{neu}})(p_1\eta_{1,\text{dir}} + \eta_{1,\text{neu}})} \right|.$$

DISCRETE ANALYSIS OF SWR FOR A DIFFUSION REACTION PROBLEM

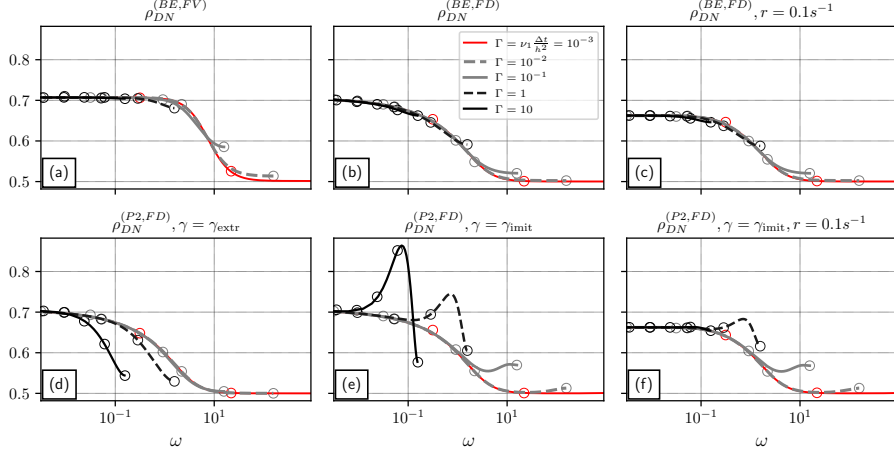


FIGURE 4.1. Interactions between space and time discretisations with Dirichlet-Neumann transmission operators. The relative importance of time and space schemes are characterised by the parabolic Courant number $\Gamma = \nu_1 \frac{\Delta t}{h^2}$: as $\Gamma \rightarrow 0$ (in red), the semi-discrete in space case is recovered, whereas the convergence rate gets closer to the semi-discrete in time setting when $\Gamma \rightarrow \infty$.

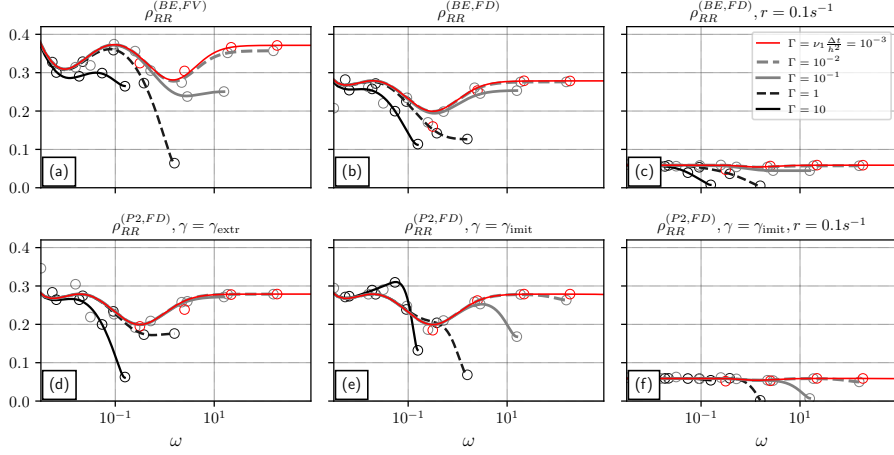


FIGURE 4.2. Convergence factor for different combinations of space and time discretisation schemes, with Robin *two-sided* transmission operators optimised in the semi-discrete in space setting (see Section 5.2). Several values of $\Gamma = \nu_1 \frac{\Delta t}{h^2}$ are compared. The reference red curve corresponds to the very small value $\Gamma = 10^{-3}$ (i.e. almost semi-discrete in space). The reaction coefficient r is set to 0, except in the right column ($r = 0.1$). The extrapolation is $\gamma_{extr} = z - \beta(z - 1)$ whereas the imitation of the scheme is $\gamma_{imit} = \gamma_{extr} - \beta(\beta - 1)^2(z - 1)^2$.

The operators η , which depend on the space discretisation, are given in Table 3.1, and the frequency variables are given in Table 3.2. A semi-discrete or fully-discrete setting is thus characterized by a particular interface operator η_j^{Space} and frequency variable s_d^{Time} . Using s_d^{P2} here amounts to neglecting the operator γ . We instead use for $\rho_{RR}^{(P2, \cdot)}$ an other expression based on subsection 3.1.3.

Section 5.2 will detail the optimisation of the convergence rate with Robin two-sided interface conditions and compare the discrete and semi-discrete cases. First results are shown in Figure 4.2 which presents the discrete convergence rates with several discretisations, reaction coefficients r and parabolic Courant number Γ . For each discretisation and reaction coefficient, Robin parameters are fixed as the optimal parameters for a semi-discrete in space setting, in order to focus on the effect of changing Γ . It is seen on this figure that the convergence speed is accelerated by Backward Euler (a,b,c) when Γ increases. When using Padé time scheme (d, e, f) the interaction with the finite difference scheme drastically depends on γ . In the right column, the presence of a reaction coefficient $r > 0$ accelerates the convergence.

The operator of projection γ becomes more important as Γ increases. However, unlike with Dirichlet-Neumann boundary conditions, the convergence is not slowed down by γ .

5. Numerical examples and optimisation of convergence rates

5.1. Comparison between numerical and theoretical convergence rates

Figures 3.2, 3.4, 4.1, 4.2 include circles that represent frequencies obtained in numerical simulations³. It is seen that the numerical simulation fits the theoretical convergence rates. In Figure 3.4 for $r = 0 \text{ s}^{-1}$ there are significant differences between the theoretical prediction with $h = 10^{-1} \text{ m}$ with FD and FV. For lower frequencies, this comes from the limited size of the space domains (100 vertical levels are used in each Ω_j : the domains are smaller if h is smaller) In the highest frequencies, the difference comes from the time discretisation. Figure 3.4 uses $\Delta t = 10^{-2} \text{ s}$ and 10^5 time steps to be close to a semi-discrete in space setting. In Figures 4.1 and 4.2 there are 10^4 time steps and 100 vertical levels are used in each Ω_j . The differences between the theoretical analysis and the numerical simulation come from the size of the time window. Other parameters are given in legend of Figure 5.1.

Note that for all the numerical experiments (including those in next section) we tried to obtain a robust estimation of the convergence rate by performing 10 simulations, each one being initialized with $e^{k=0}$ as a white noise. Schwarz algorithm is applied to each of these 10 simulations. The convergence rate is then computed as the rate of reduction of the standard deviation of the quantity $|p_1 \hat{e}_2^k + \nu_2 \hat{\phi}_2^k|$ over the 10 instances.

5.2. Optimisation of the two-sided Robin interface conditions

Having an accurate description of the discrete convergence rate is useful to maximize the convergence speed. One way to do so stems from the optimised Schwarz methods framework [e.g. 14]. In the present study we consider an optimisation based on the two-sided Robin interface conditions defined in §2.3. Those interface conditions introduce two free parameters p_1, p_2 which can be chosen to minimise the convergence rate:

$$(p_1, p_2) = \underset{(q_1, q_2) \in \mathbb{R}^2}{\operatorname{argmin}} \max_{\omega_{\min} \leq \omega \leq \omega_{\max}} \rho_{RR}^{(\cdot, \cdot)}(\omega; q_1, q_2). \quad (5.1)$$

Depending on which $\rho_{RR}^{(\cdot, \cdot)}$ is used, the optimal (p_1, p_2) may differ.

Figure 5.1 compares the solutions of (5.1) with convergence rates obtained through continuous, semi-discrete in time and discrete analyses. It illustrates how taking a discretisation into account in (5.1) affects the convergence speed of Schwarz algorithms. Several comments can be drawn (theoretical $\rho^{(\cdot, \cdot)}$ are referred to as “prediction” in the following sentences):

³The code used is available in the Zenodo archive (<https://doi.org/10.5281/zenodo.6324930>, [9])

TABLE 5.1. Ratio of the L2 norms between consecutive iterations ($k = 1, 2$) in cases shown in Figure 5.1. Left (resp. right) parts of the cells correspond to the BE (resp. P2) implementation and to the left (resp. right) of Figure 5.1. The first three lines of this Table are obtained with the FV implementation.

Optimised $\rho_{RR}^{(\cdot, \cdot)}$ (left right)	$\frac{\ p_1 e_2^{k=2} + \phi_2^{k=2}\ _2}{\ p_1 e_2^{k=1} + \phi_2^{k=1}\ _2}$ (with BE P2)	Figure 5.1 color
$\rho_{RR}^{(c,c)} \rho_{RR}^{(c,c)}$	0.32 0.32	green
$\rho_{RR}^{(BE,c)} \rho_{RR}^{(P2,c)}$	0.28 0.29	red
$\rho_{RR}^{(BE,FV)} \rho_{RR}^{(P2,FV)}$	0.28 0.30	black
$\rho_{RR}^{(BE,FD)} \rho_{RR}^{(P2,FD)}$	0.23 0.23 (FD)	blue

- The first thing to notice is that predictions (triangles) are close to corresponding observed values (solid lines of the same color): they accurately fit, except for high frequencies in the continuous or semi-discrete cases.
- For high frequencies, the convergence rate predicted by the continuous analysis significantly differs from the actual convergence rate, which is here smaller than the prediction. For lower frequencies, the discretisations accurately describe the continuous equations. Similarly to Figure 4.1, changing the time step would shift the frequencies for which the continuous equation is well represented. As in the upper part of Figure 3.4 decreasing the space step would reduce the range of frequencies for which the continuous and semi-discrete in space convergence rate differ since r is small.
- The discrete analysis provides a better convergence (the maximum attained by the curves “Discrete” are smaller than the maximum attained by the other analyses) and Robin parameters change significantly between the discrete and continuous cases.
- The optimised convergence is faster for finite differences with $k_c = 0$ than for finite volumes. It is also the case for Dirichlet-Neumann in Figure 4.1 and Figure 3.4 indicates that this comes from the discretisation of the flux.
- The optimal Robin parameters minimise a 3-point equi-oscillation. If the prediction differs from the observed convergence at one of the equi-oscillation points then the minimisation can be refined.
- Table 5.1 gives the convergence rate of the L^2 norm in the time domain for each simulation of Figure 5.1. The maximum of $\rho_{RR}^{(\cdot, \cdot)}$ is an upper bound of the L^2 convergence rate and it is seen that the discrete analysis provides as well a better convergence in the time domain. It was checked that the convergence is linear for our choice of time window. For shorter time windows, the convergence is superlinear as shown in the case of SWR with Dirichlet boundary conditions in [10].

The choice was made here to illustrate the use of discrete analysis on Robin *two sided* transmission operators, but an optimisation could of course also be performed on a relaxation parameter within Dirichlet-Neumann interface conditions [e.g. 16, 22]. We quantitatively checked (not shown) that for values of ν_1, ν_2 varying in a range from 10^{-2} to 2 the results obtained are consistent with the one shown in Figure 5.1 for particular values of ν_1, ν_2 . Our results hence seem quite robust to the values of these parameters.

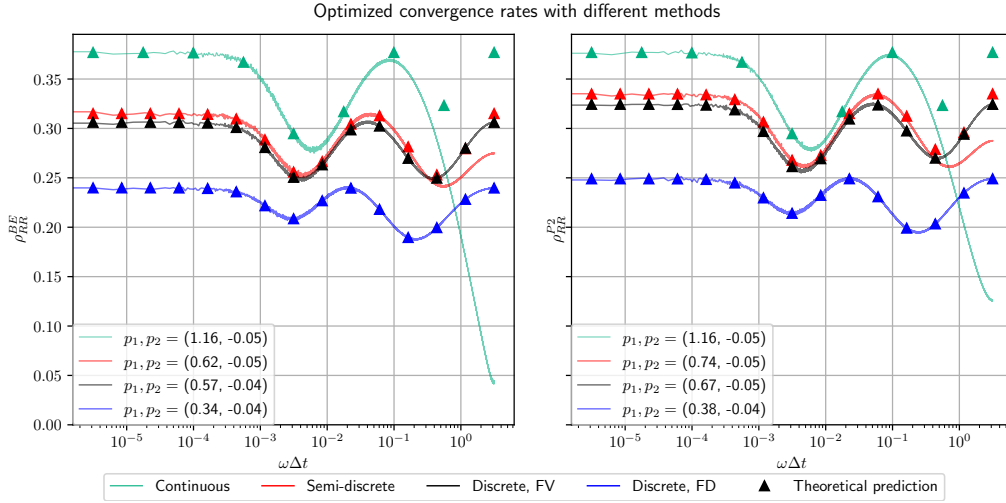


FIGURE 5.1. Comparison of theoretical (triangles) and observed (solid lines) convergence rates with Robin-Robin interface conditions. Theoretical values correspond to $\rho_{RR}^{(c,c)}(p_1, p_2)$ (green), $\rho_{RR}^{(\text{Time},c)}(p_1, p_2)$ (red), $\rho_{RR}^{(\text{Time},\text{FV})}(p_1, p_2)$ (black) and $\rho_{RR}^{(\text{Time},\text{FD})}(p_1, p_2)$ (blue), with “Time” being BE (left panel) or P2 (right panel). The actual values of p_1, p_2 are chosen to solve the min-max optimisation problem of the corresponding convergence rate. Solid lines are Fourier-transformed observed convergence rates obtained by implementing SWR in a numerical code, with the finite difference scheme ($\kappa_c = 0$) for the blue line and the finite volume scheme in the other cases. Parameter values are $\nu_1 = 0.5 \text{ m}^2\text{s}^{-1}$, $\nu_2 = 1 \text{ m}^2\text{s}^{-1}$, $h = 1 \text{ m}$, $r = 10^{-3} \text{ s}^{-1}$, $\Delta t = 1 \text{ s}$ and $\omega \Delta t \leq \pi$. For Padé time scheme, $\gamma = \gamma_{\text{extr}}$. There are 100 space levels in each domain and 10^6 time steps.

6. Conclusion

In this paper, we studied an iterative Schwarz method defined for non-overlapping diffusion-reaction problems with discontinuous coefficients. We analytically examined the behavior of the discrete convergence rates of the iterative process for different spatial and temporal discretisations of the problem and compared it to the ones obtained in the conventional continuous case. In particular we showed that the discretisation of the interface conditions has a significant impact on the efficiency of the method. For example the standard ghost-point method used for the finite difference discretisation of Neumann conditions significantly slows down the convergence speed for high frequencies. As far as the time dimension is concerned, when a simple one-step time-stepping scheme is used the impact of the temporal discretisation on the convergence can be easily obtained from the continuous analysis via a change of frequency variable. However for more advanced multi-step schemes the algebra is more tedious because higher-order differential equations must be considered to determine the convergence rate. In this case we also showed that the projection operator required to provide the boundary data at the intermediate steps must be carefully chosen not to compromise the convergence speed. This aspect has been discussed for a diagonally implicit Runge-Kutta scheme and a two-step “Padé” scheme.

A discrete analysis provides a convergence rate more representative of the behavior observed in actual numerical experiments. Knowledge of the discrete convergence rate is thus advantageous for techniques aimed at optimising the speed of convergence either through approximation of the absorbing conditions or through a relaxation parameter weighting two or more successive iterates. We have

illustrated this aspect in the particular case of zeroth-order approximation of the absorbing conditions (i.e. using two-sided Robin-Robin interface conditions).

In future work the methodology developed in the present paper will be applied to problems with more complex interface conditions (e.g. in the presence of turbulent boundary layers) like the ones arising from wall laws in fluid dynamics. With applications to multi-physics settings in mind the approach presented in this paper can also be used to analyse the case of different time and space discretisations in each subdomain.

Appendix A. A finite volume scheme based on quadratic spline reconstruction

We present here a finite volume alternative to the standard finite difference scheme introduced in section 3.2.1. We construct a scheme based on quadratic splines. This scheme offers the advantage to naturally handle the transmission conditions between the two non-overlapping domains and to guarantee that the converged solution is similar to the monolithic solution of the problem. In this appendix we drop the j subscript to denote subdomains for the sake of clarity. As described in Figure 3.3, we consider control volumes delimited by x_m and x_{m+1} such that $h = x_{m+1} - x_m$ and the solution $\bar{u}_{m+\frac{1}{2}}$ has to be interpreted in a finite volume sense, i.e. $\bar{u}_{m+\frac{1}{2}} = \frac{1}{h} \int_{x_m}^{x_{m+1}} u(x) dx$.

We suppose here that the subgrid reconstruction $u(x)$ on a volume centered at $x = x_{m+\frac{1}{2}}$ is given by a quadratic polynomial:

$$u(x) = \mathcal{S}_{m+\frac{1}{2}}(x - x_{m+\frac{1}{2}}) \quad \text{with } x - x_{m+\frac{1}{2}} \in \left[-\frac{h}{2}; \frac{h}{2}\right]$$

$$\mathcal{S}_{m+\frac{1}{2}}(\xi) = r_{m+\frac{1}{2},2}\xi^2 + r_{m+\frac{1}{2},1}\xi + r_{m+\frac{1}{2},0}.$$

Consistent with (3.10) in section 3.2, we note ϕ_m^{FV} the approximation of the derivative of u at the interface between volumes $m - \frac{1}{2}$ and $m + \frac{1}{2}$. The coefficients $r_{m+\frac{1}{2},p}$ in $\mathcal{S}_{m+\frac{1}{2}}(\xi)$ are chosen to satisfy the following constraints:

- (1) $\frac{1}{h} \int_{-h/2}^{h/2} \mathcal{S}_{m+\frac{1}{2}}(\xi) d\xi = \bar{u}_{m+\frac{1}{2}}$
- (2) $\partial_\xi \mathcal{S}_{m+\frac{1}{2}}(-h/2) = \phi_m^{\text{FV}}$
- (3) $\partial_\xi \mathcal{S}_{m+\frac{1}{2}}(h/2) = \phi_{m+1}^{\text{FV}}$.

Those constraints, imposing the continuity of ϕ between two neighboring volumes and the consistency with $\bar{u}_{m+\frac{1}{2}}$, provide $r_{m+\frac{1}{2},p}$ coefficients such that:

$$\mathcal{S}_{m+\frac{1}{2}}(\xi) = \bar{u}_{m+\frac{1}{2}} + \frac{\phi_{m+1}^{\text{FV}} + \phi_m^{\text{FV}}}{2} \xi + \frac{\phi_{m+1}^{\text{FV}} - \phi_m^{\text{FV}}}{2h} \left(\xi^2 - \frac{h^2}{12} \right). \quad (\text{A.1})$$

The last step amounts to impose the continuity of the solution at cell interfaces, i.e. $\mathcal{S}_{m-\frac{1}{2}}\left(\frac{h}{2}\right) = \mathcal{S}_{m+\frac{1}{2}}\left(-\frac{h}{2}\right)$, to obtain

$$\frac{1}{6}\phi_{m-1}^{\text{FV}} + \frac{2}{3}\phi_m^{\text{FV}} + \frac{1}{6}\phi_{m+1}^{\text{FV}} = \frac{\bar{u}_{m+\frac{1}{2}} - \bar{u}_{m-\frac{1}{2}}}{h} \quad (\text{A.2})$$

which corresponds to a tridiagonal problem to solve to get ϕ_m^{FV} and then the second-order derivative via (3.10). This scheme was also used for example in [25] to discretise vertical advection in an oceanic

model. Note that using coefficients $\frac{1}{12}$ instead of $\frac{1}{6}$ and $\frac{5}{6}$ instead of $\frac{2}{3}$ in (A.2) would lead to a fourth-order accurate compact scheme [e.g. 18].

Now that we have presented the numerical scheme of interest, we apply it to the equation satisfied by the error. Considering (3.10) and the equations satisfied by the errors \bar{e}_m interpreted in a finite volume sense we end up with

$$(\partial_t + r)\bar{e}_{m+\frac{1}{2}} = \frac{\nu}{h} (\phi_m^{\text{FV}} - \phi_{m-1}^{\text{FV}}) \quad (\text{A.3})$$

$$(\partial_t + r)\bar{e}_{m-\frac{1}{2}} = \frac{\nu}{h} (\phi_{m+1}^{\text{FV}} - \phi_m^{\text{FV}}) \quad (\text{A.4})$$

which, when combined with (A.2), leads to

$$(\partial_t + r) \left(\frac{1}{6}\phi_{m-1}^{\text{FV}} + \frac{2}{3}\phi_m^{\text{FV}} + \frac{1}{6}\phi_{m+1}^{\text{FV}} \right) - \frac{\nu}{h^2} (\phi_{m+1}^{\text{FV}} - 2\phi_m^{\text{FV}} + \phi_{m-1}^{\text{FV}}) = 0.$$

Acknowledgement

We thank the two anonymous reviewers whose suggestions helped improve and clarify this manuscript.

Code availability

The code used to generate Figures and Table 5.1 is available in a Zenodo archive (<https://doi.org/10.5281/zenodo.6324930>, [9]).

References

- [1] M. D. Al-Khaleel and S.-L. Wu. Quasi-overlapping Semi-discrete Schwarz Waveform Relaxation Algorithms: The Hyperbolic Problem. *Comput. Methods Appl. Math.*, 20(3):397–417, 2020.
- [2] R. Alexander. Diagonally Implicit Runge–Kutta Methods for Stiff O.D.E.’s. *SIAM J. Numer. Anal.*, 14(6):1006–1021, 1977.
- [3] P. Azimzadeh and P. A. Forsyth. Weakly Chained Matrices, Policy Iteration, and Impulse Control. *SIAM J. Numer. Anal.*, 54(3):1341–1364, 2016.
- [4] R. J. Beerends, H. G. ter Morsche, J. C. van den Berg, and E. M. van de Vrie. *Fourier and Laplace Transforms*. Cambridge University Press, 2003.
- [5] P.-M. Berthe. *Méthodes de décomposition de domaine de type relaxation d’ondes optimisées pour l’équation de convection-diffusion instationnaire discrétisée par volumes finis*. PhD thesis, Paris 13, 2013. Thèse de doctorat dirigée par Omnes, P. et Japhet, C. Mathématiques appliquées Paris 13 2013.
- [6] P.-M. Berthe, C. Japhet, and P. Omnes. Space–Time Domain Decomposition with Finite Volumes for Porous Media Applications. In *Domain Decomposition Methods in Science and Engineering XXI*, pages 567–575. Springer, 2014.
- [7] N. F. Britton et al. *Reaction-diffusion equations and their applications to biology*. Academic Press Inc., 1986.
- [8] F. Caetano, M. J. Gander, L. Halpern, and J. Szeftel. Schwarz waveform relaxation algorithms for semilinear reaction-diffusion equations. *Netw. Heterog. Media*, 5(3):487–505, 2010.

- [9] Simon Clement. Code for Discrete analysis of SWR for a diffusion reaction problem with discontinuous coefficients, 2022. <https://zenodo.org/record/6324930>.
- [10] M. J. Gander. A waveform relaxation algorithm with overlapping splitting for reaction diffusion equations. *Numer. Linear Algebra Appl.*, 6(2):125–145, 1999.
- [11] M. J. Gander and L. Halpern. Optimized Schwarz Waveform Relaxation Methods for Advection Reaction Diffusion Problems. *SIAM J. Numer. Anal.*, 45(2):666–697, 2007.
- [12] M. J. Gander, L. Halpern, F. Hubert, and S. Krell. Optimized Overlapping DDFV Schwarz Algorithms. In *Finite Volumes for Complex Applications IX - Methods, Theoretical Aspects, Examples*, pages 365–373. Springer, 2020.
- [13] M. J. Gander, L. Halpern, and M. Kern. A Schwarz Waveform Relaxation Method for Advection—Diffusion—Reaction Problems with Discontinuous Coefficients and Non-matching Grids. In *Domain Decomposition Methods in Science and Engineering XVI*, pages 283–290. Springer, 2007.
- [14] M. J. Gander, L. Halpern, and F. Nataf. Optimal Schwarz waveform relaxation for the one dimensional wave equation. *SIAM J. Numer. Anal.*, 41(5):1643–1681, 2003.
- [15] M. J. Gander, F. Hubert, and S. Krell. Optimized Schwarz Algorithms in the Framework of DDFV Schemes. In *Domain Decomposition Methods in Science and Engineering XXI*, pages 457–466. Springer, 2014.
- [16] M. J. Gander, F. Kwok, and B. C. Mandal. Dirichlet–Neumann waveform relaxation methods for parabolic and hyperbolic problems in multiple subdomains. *BIT Numer. Math.*, 61(1):173–207, 2021.
- [17] R. D. Haynes and K. Mohammad. Fully Discrete Schwarz Waveform Relaxation on Two Bounded Overlapping Subdomains. In *Domain Decomposition Methods in Science and Engineering XXV*, pages 159–166. Springer, 2020.
- [18] M. H. Kobayashi. On a Class of Padé Finite Volume Methods. *J. Comput. Phys.*, 156(1):137–180, 1999.
- [19] F. Lemarié. *Algorithmes de Schwarz et couplage océan-atmosphère*. Theses, Université Joseph-Fourier - Grenoble I, 2008.
- [20] F. Lemarié, L. Debreu, G. Madec, J. Demange, J. M. Molines, and M. Honnorat. Stability constraints for oceanic numerical models: implications for the formulation of time and space discretizations. *Ocean Modelling*, 92:124–148, 2015.
- [21] G. Manfredi and M. Ottaviani. Finite-difference schemes for the diffusion equation. In *Dynamical Systems, Plasmas and Gravitation*, pages 82–92. Springer, 1999.
- [22] A. Monge and P. Birken. A Multirate Neumann–Neumann Waveform Relaxation Method for Heterogeneous Coupled Heat Equations. *SIAM J. Sci. Comput.*, 41(5):S86–S105, 2019.
- [23] F. Nataf. Recent Developments on Optimized Schwarz Methods. In *Domain Decomposition Methods in Science and Engineering XVI*, pages 115–125. Springer, 2007.

- [24] E. Nourtier-Mazauric and E. Blayo. Towards efficient interface conditions for a Schwarz domain decomposition algorithm for an advection equation with biharmonic diffusion. *Appl. Numer. Math.*, 60(1):83–93, 2010.
- [25] A. F. Shchepetkin. An adaptive, Courant-number-dependent implicit scheme for vertical advection in oceanic modeling. *Ocean Modelling*, 91:38–69, 2015.
- [26] J. Smoller. *Shock waves and reaction-diffusion equations*, volume 258 of *Grundlehren der Mathematischen Wissenschaften*. Springer, 1983.
- [27] S. Thery, C. Pelletier, F. Lemarié, and E. Blayo. Analysis of Schwarz waveform relaxation for the coupled Ekman boundary layer problem with continuously variable coefficients. *Numer. Algorithms*, 2021.
- [28] N. Wood, M. Diamantakis, and A. Staniforth. A monotonically-damping second-order-accurate unconditionally-stable numerical scheme for diffusion. *Quarterly Journal of the Royal Meteorological Society*, 133(627):1559–1573, 2007.
- [29] S.-L. Wu and M. D. Al-Khaleel. Semi-discrete Schwarz waveform relaxation algorithms for reaction diffusion equations. *BIT Numer. Math.*, 54(3):831–866, 2014.
- [30] S.-L. Wu and M. D. Al-Khaleel. Optimized waveform relaxation methods for RC circuits: discrete case. *ESAIM: M2AN*, 51(1):209–223, 2017.
- [31] A. Zisowsky and M. Ehrhardt. Discrete transparent boundary conditions for parabolic systems. *Math. Comput. Modelling*, 43(3):294–309, 2006.